AGU PUBLICATIONS

JGR

Journal of Geophysical Research: Oceans

RESEARCH ARTICLE

10.1002/2015JC011514

Key Points:
- Downwelling-favorable winter storms result in storm surges along the Beaufort Sea coast
- Cross-slope pressure gradient drives barotropic flow enhancing baroclinic along-slope current
- Downwelling of the Pacific Winter and Atlantic Water was observed

Correspondence to:
I. A. Dmitrenko,
igor.dmitrenko@umanitoba.ca

Citation:
Dmitrenko, I. A., S. A. Kirillov, A. Forest, Y. Gratton, D. L. Volkov, W. J. Williams, J. V. Lukovich, C. Belanger, and D. G. Barber (2016), Shelfbreak current over the Canadian Beaufort Sea continental slope: Wind-driven events in January 2005, *J. Geophys. Res. Oceans*, *121*, 2447–2468, doi:10.1002/2015JC011514.

Received 7 DEC 2015
Accepted 15 MAR 2016
Accepted article online 18 MAR 2016
Published online 9 APR 2016

Shelfbreak current over the Canadian Beaufort Sea continental slope: Wind-driven events in January 2005

Igor A. Dmitrenko[1], Sergei A. Kirillov[1], Alexandre Forest[2], Yves Gratton[3], Denis L. Volkov[4,5], William J. Williams[6], Jennifer V. Lukovich[1], Claude Belanger[3], and David G. Barber[1]

[1]Centre for Earth Observation Science, University of Manitoba, Winnipeg, Manitoba, Canada, [2]Golder Associates Ltd. Québec, Québec, Canada, [3]Institut National de la Recherche Scientifique - Eau Terre Environnement, Québec, Québec, Canada, [4]Cooperative Institute for Marine and Atmospheric Studies, University of Miami, Miami, Florida, USA, [5]NOAA, Atlantic Oceanographic and Meteorological Laboratory, Miami, Florida, USA, [6]Institute of Ocean Sciences, Fisheries and Oceans Canada, Sidney, British Columbia, Canada

Abstract The shelfbreak current over the Beaufort Sea continental slope is known to be one of the most energetic features of the Beaufort Sea hydrography. In January 2005, three oceanographic moorings deployed over the Canadian (eastern) Beaufort Sea continental slope simultaneously recorded two consecutive shelfbreak current events with along-slope eastward bottom-intensified flow up to 120 cm s^{-1}. Both events were generated by the local wind forcing associated with two Pacific-born cyclones passing north of the Beaufort Sea continental slope toward the Canadian Archipelago. Over the mooring array, the associated westerly wind exceeded 15 m s^{-1}. These two cyclones generated storm surges along the Beaufort Sea coast with sea surface height (SSH) rising up to 1.4 m following the two westerly wind maxima. We suggest that the westerly along-slope wind generated a surface Ekman onshore transport. The associated SSH increase over the shelf produced a cross-slope pressure gradient that drove an along-slope eastward geostrophic current, in the same direction as the wind. This wind-driven barotropic flow was superimposed on the background baroclinic bottom-intensified shelfbreak current that consequently amplified. Summer-fall satellite altimetry data for 1992–2013 show that the SSH gradient in the southeastern Beaufort Sea is enhanced over the upper continental slope in response to frequent storm surge events. Because the local wind forcing and/or sea-ice drift could not explain the reduction of sea-ice concentration over the Beaufort Sea continental slope in January 2005, we speculate that wind-driven sea level fluctuations may impact the sea-ice cover in winter.

1. Introduction

The Canadian Beaufort Sea continental slope in the eastern Beaufort Sea with shelfbreak at ~80 m depth is bordered by the Beaufort Sea continental shelf of about 120 km width to the south, Amundsen Gulf to the east, and Mackenzie Canyon to the west (Figure 1). It is well known that the shelfbreak jet is an important feature of the ocean circulation pattern over the adjacent western (Alaskan) Beaufort Sea continental slope (Figure 1). This along-slope current has an average velocity of about 15 cm s^{-1} and flows eastward toward the Canadian Archipelago as a bottom-intensified narrow (10–15 km width) jet, trapped by the shelfbreak [*Nikolopoulos et al.*, 2009]. It advects the Pacific-origin summer water near the shelfbreak (at depths shallower than 100 m) and Pacific-origin winter water at deeper depths (to roughly 150 m) [e.g., *Pickart*, 2004; *Nikolopoulos et al.*, 2009; *von Appen and Pickart*, 2012]. Below this resides the warm and salty Atlantic Water advected in the same direction as the Pacific Water by the Atlantic Water circumpolar boundary current [e.g., *Rudels et al.*, 1994; *McLaughlin et al.*, 2002, 2004].

It is reasonable to suggest that over the eastern (Canadian) Beaufort Sea slope, the Beaufort shelfbreak current flows further east toward Fram Strait as an extension of the western Beaufort shelfbreak current, presumably carrying a significant amount of Pacific Water further eastward. This is consistent with traces of the Pacific Water found in Fram Strait and along northeast Greenland [*Jones et al.*, 1998, 2003; *Rudels et al.*, 2004]. A yearlong velocity record from a mooring deployed in 1987–1988 over the upper continental shelf (70°57′N, 225°31′E, 180 m deep, ~5 km from the shelf edge) in the Canadian Beaufort Sea shows the mean westward (~270°) depth-intensified flow increasing from 3 cm s^{-1} at 35 m to 11 cm s^{-1} at 130 m [*Kulikov*

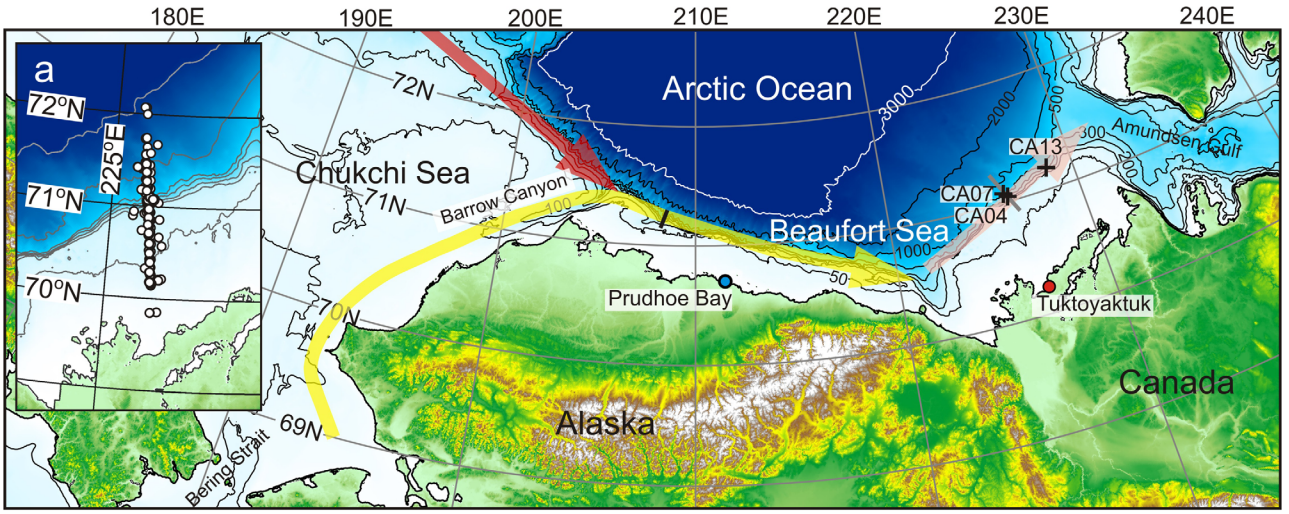

Figure 1. Map of the Chukchi and Beaufort seas with location of the ArcticNet moorings depicted with black numbered crosses. Blue and red dots indicate the tide gauge in Prudhoe Bay and Tuktoyaktuk, respectively. Orange, yellow, and pink arrows show circulation with shelfbreak jet over the Chukchi Sea and western and eastern Beaufort Sea, respectively. Black line at ~208°E depicts mooring array maintained downstream of the Barrow Canyon by the WHOI. Gray line shows location of the CTD cross-slope transect taken in July 2004. (a) CTD stations occupied during summer 2002–2011 and used for compiling the long-term summer mean cross-slope CTD section following ~126°E (Figures 12c and 12d).

et al., 1998]. This flow represented the dominant mode, but the second eastward (~70°) mode with velocities exceeding 10 cm s^{-1} was observed in ~4% of all hourly velocity measurements [*Kulikov et al*., 1998]. Yearlong velocity data from a mooring deployed in 1995–1996 over the lower continental slope (70°33′N, 223°11′E, 765 m deep, ~20 km from the shelfbreak) in the eastern Beaufort Sea also revealed a bimodal along-slope distribution [*Williams et al*., 2006]. The eastward middepth flow (~70°) of ~9 cm s^{-1} was observed in ~10% of all velocity measurements. The opposite westward flow of ~5 cm s^{-1} occurred in ~15% of observations. Overall, the along-shelf flow accounts for 76% of the velocity variance [*Williams et al*., 2006]. Recent current measurements over the upper slope (~4 km from the shelf edge and 150 m deep) from 2009 to 2012 further confirmed the existence of a mean northeastward flow carrying Pacific Water over the depth range from 50 m to the bottom, as would be expected from the advection by a shelfbreak jet originating from the Alaskan Beaufort Sea [*Forest et al*., 2015].

The ocean dynamics over the Beaufort Sea continental slope is known to be highly sensitive to wind forcing [e.g., *Williams et al*., 2006; *Pickart et al*., 2009, 2011]. Synoptically, the shelfbreak current can reverse and flow to the west in response to wind forcing [*Nikolopoulos et al*., 2009; *Pickart et al*., 2013a]. In the southern Canada Basin, these events are usually associated with the occurrence of upwelling storms due to easterly or northeasterly winds that are associated with the Aleutian low storms generated to the south [*Pickart et al*., 2009]. Under such conditions, the usually eastward-flowing Pacific Water shelfbreak jet reverses to the west, and Pacific and Atlantic Waters are brought onto the shelf and the isohalines shoal toward the shore. The upwelling events have been reported for both the western [*Nikolopoulos et al*., 2009; *Pickart et al*., 2009, 2011, 2013a, 2013b; *Schulze and Pickart*, 2012] and the eastern [*Carmack and Kulikov*, 1998; *Kulikov et al*., 1998; *Williams et al*., 2006, 2008; *Jackson et al*., 2015] Beaufort Sea continental slope.

The wind-forced downwelling over the Beaufort Sea continental slope is expected for westerly winds because the offshore transport develops at depth in response to the onshore Ekman transport near the surface [e.g., *Yang*, 2009]. Over the continental slope of the Canadian Beaufort Sea, westerly winds are associated with cyclonic atmospheric circulation, which dominates in this region ~30% of time throughout the year [*Asplin et al*., 2009]. The seasonal occurrence of cyclonic atmospheric circulation is ~17% and 40% for November–April and May–October, respectively.

The downwelling events possibly drive an enhanced shelfbreak current [*Nikolopoulos et al*., 2009; *Pickart et al*., 2013a; *Forest et al*., 2015]. In contrast to upwelling, relatively little is known about downwelling, particularly along the continental slope of the Canadian Beaufort Sea. Individual downwelling events have been observed in mooring records from the eastern Beaufort slope [*Melling*, 1993] and near the shelf [*Williams et al*., 2008]. More recently, they have been hypothesized to play a key role in the shelf-slope transport of

resuspended material along with dense water cascading [*Forest et al*., 2015]. Despite the possible role of downwelling in facilitating the along-slope transport, very little is known about the associated oceanographic processes and implications due to a lack of direct observations during downwelling-favorable storms.

This paper is focused on the oceanic response to the downwelling-favorable atmospheric forcing over the eastern Beaufort continental slope. We investigate two exceptionally strong downwelling-favorable storms and associated major shelfbreak current intensifications observed over the Canadian Beaufort Sea continental slope in January 2005 in response to Pacific-born cyclones, which subsequently propagated seaward off the shelfbreak to the Canadian Archipelago. We note that these two Pacific-born storms are different from those resulting in upwelling over the western Beaufort Sea continental slope. Upwelling-favorable storms described by *Pickart et al*. [2009] were characterized by deep and meridionally elongated Aleutian low-pressure systems that originated from the Aleutian Arc and Alaskan Peninsula in fall, and migrated northeastward [*Pickart et al*., 2009, Figure 8]. By contrast, in the present study, Pacific-born storms were initially generated over the northwest Pacific Ocean. They approached the eastern Beaufort Sea from the west, first moving northward over Siberia to the Arctic Ocean and then passing north of the Beaufort Sea continental slope toward the Canadian Archipelago. Therefore, according to classification of *Hudak and Young* [2002], these storms are referred to as the downwelling-favorable Arctic storms [*Pickart et al*., 2009]. Overall, 58% of storms over the southern Beaufort Sea are classified as the Arctic storms with a mean reoccurrence of approximately eight storms per season [*Hudak and Young*, 2002]. During December–February, over the Canadian Beaufort Sea continental slope, storms generate downwelling-favorable cyclonic winds with a percent frequency of ~30% based on data for the period 1979–2008 [*Serreze and Barrett*, 2011].

Here we show how these individual Pacific-born storms with westerly winds exceeding 15 m s^{-1} affected hydrography and sea level along the coast, in a manner consistent with downwelling. In particular, the isohalines of the upper Atlantic Water deepened in the vicinity of the upper slope, and there was a depth-intensified shelfbreak jet that headed eastward with velocities of up to 120 cm s^{-1}.

The paper is structured as follows. Section 2 describes the observational data and provides motivation for our focus on two downwelling-favorable storms in this study. Section 3 provides an overview of the atmospheric forcing and ice conditions, and then it presents temperature, salinity, and velocity data from a mooring array deployed over the eastern Beaufort continental slope, as well as sea surface height (SSH) measurements along the Beaufort Sea coast. Section 4.1 puts the findings into the context of the long-term mean thermohaline structure and examines the sources of water masses over the upper continental slope. Section 4.2 examines the role of wind-driven downwelling in conditioning the thermohaline structure and shelfbreak current over the Canadian Beaufort Sea continental slope. Section 4.3 discusses the sea-ice distribution observed during a downwelling storm in a context of sea level deformation extending our analysis onto the ice-free summer period when satellite altimetry data are available. Finally, section 5 concludes the analysis and discusses limitations.

2. Data and Methods

We used oceanographic data (CTD and velocity records) from three moorings deployed over the upper Canadian Beaufort Sea continental slope (Figure 1). Moorings CA04-04 and CA07-04 were deployed from 7 and 8 September 2004, respectively, to 4 September 2005 at ~226°E across the upper continental slope at 306 m depth (CA04) and 490 m depth (CA07). Mooring CA13-03 was deployed ~90 km eastward at 300 m depth from 9 October 2003 to 4 September 2005. All moorings carried a combination of (i) 300 kHz up-looking Workhorse Sentinel acoustic Doppler current profilers (ADCPs) by Teledyne RD Instruments (~100 m depth), (ii) Sea-Bird Electronics, Inc., SBE-37s with conductivity-temperature-depth (CTD) sensors (moorings CA07 and CA13) or ALEC ACT-HR by JFE Advantech Co., Ltd with temperature and conductivity sensors (CA04) at the near-surface layer (17–49 m), and (iii) Aanderaa Instruments Recording Current Meters (RCM-11s) with CTD and Doppler velocity sensors at the upper Atlantic Water layer (174–216 m) and at 387 m (CA07 only). The ADCPs at CA04 and CA07 were not equipped with pressure sensors, and the deployment depth was determined by tracking the water-air interface on the acoustic backscatter maximum with accuracy of ~±4 m. The mooring description is summarized in Table 1.

Table 1. Mooring Description

	CA04-04	CA07-04	CA13-03
Latitude, N	71°05.146′	71°08.944′	71°21.356′
Longitude, E	226°16.729′	226°6.365′	228°38.176′
Depth (m)	306	490	300
Deployed	7 Sep 2004	8 Sep 2004	9 Oct 2003
Recovered	4 Sep 2005	4 Sep 2005	4 Sep 2005
ADCP depth (m)	~90[a]	~85[a]	119
ADCP record (from-to)	7 Sep 2004 to 4 Sep 2005	7 Sep 2004 to 15 May 2005	9 Oct 2003 to 4 Jun 2005
SBE-37 CTD depth		17	49
SBE-37 CTD record (from-to)		7 Sep 2004 to 15 May 2005	9 Oct 2003 to 4 Sep 2005
ALEC CT depth (m)	31[a]		
ALEC CT record (from-to)	7 Sep 2004 to 4 Sep 2005		
RCM-11 depth (m)	198	184 and 387	217
RCM-11 record (from-to)	7 Sep 2004 to 29 Aug 2005[b]	8 Sep 2004 to 4 Sep 2005 and 27 Jun 2005	9 Oct 2003 to 9 Feb 2005

[a]No pressure sensor.
[b]No conductivity (salinity) data.

The length of records at the three moorings is different. For this study, we use only concurrent records from 8 September 2004 to 9 February 2005, with the exception of Figure 2 showing the 2 year long time series of kinetic energy $E = (U^2 + V^2)/2$ derived from the entire velocity record at CA13 from 9 October 2003 to 4 September 2005 (Table 1). On 13 May 2005, the CA07 mooring line slipped down the slope deepening the entire mooring structure. As a result, the near-surface SBE-37 deepened from 19 to 137 m depth. The ADCP and RCM-11 of the mooring CA13 stopped recording on 4 June 2005 and on 9 February 2005, respectively.

Among all moorings, CA13 provided the longest velocity record from October 2003 to September 2005. This time series shows that the most energetic velocity events occurred in January 2005 in a form of a

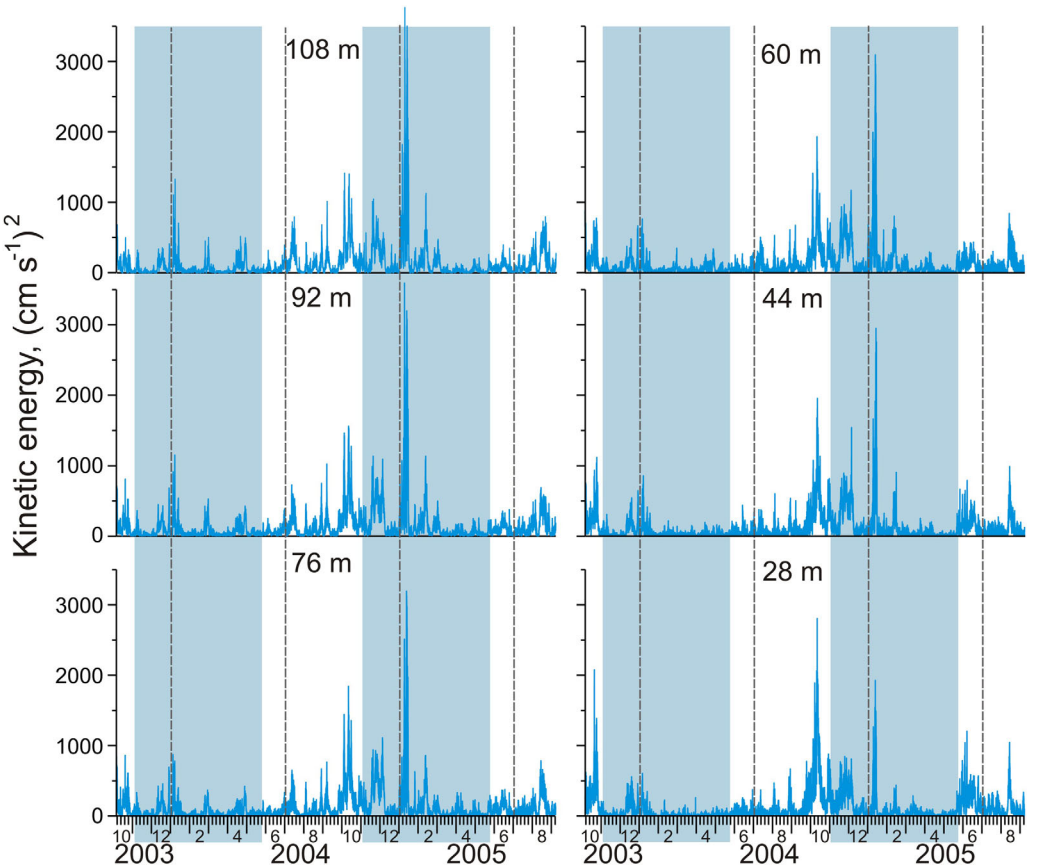

Figure 2. Time series of current kinetic energy derived from the 2 year long ADCP record at mooring CA13 for indicated water depths adopted from *Barber et al.* [2015]. Blue shading highlights occurrence of pack ice cover over the mooring location.

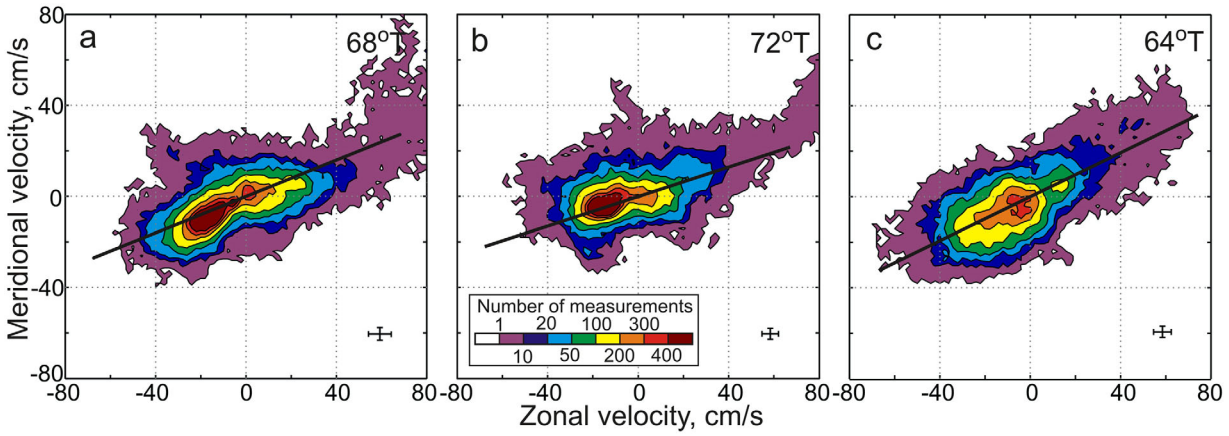

Figure 3. The scatterplot of the 24 h mean velocity measured from 8 September 2004 to 9 February 2005 by ADCP at moorings (a) CA04, (b) CA07, and (c) CA13. Black lines show the least squares regression. The error bars in the bottom right of each plot indicates velocity dispersion (±1 standard deviation) attributed to flow baroclinicity (see text for more details).

depth-intensified flow (Figure 2). A similar but less intense flow event was recorded in December 2003. In this paper, we specifically focus on the high-flow events in 2005 simultaneously recorded by all three moorings on 6–13 January 2005. During these events, velocity increased from ~30 to 126 cm s^{-1} causing the mooring line to incline. This led to a significant deepening of all instruments. For example, on 9 January 2005 at CA07, the near-surface SBE-37 deepened by ~150 m, and RCM-11 by ~120 m. For the high-flow events, depths of ADCPs at CA04 and CA07 were calculated using pressure measurements by the closest CTD. We also note that during the high-flow event on 11 January 2005 at CA04, the ADCP tilt increased to 25° (exceeding the operational range of 20°) during ~6 h when velocity was higher than 100 cm s^{-1}. At moorings CA07 and CA13, the ADCP tilt did not exceed 18° and 9°, respectively.

The velocity data from the ADCPs were obtained at ~8 m depth intervals, with a 1 h ensemble time interval and 30 pings per ensemble. The first bin was located at 10 m above the transducer. The fixed-depth CT (conductivity-temperature) and CTDs on ALEC, SBE-37s, and RCM-11s recorded data at discrete depths every 10 min, 15 min, and 1 h, respectively.

Mooring-based observations were complemented by a cross-slope CTD transect carried out between 28 June and 1 July 2004 with an SBE-911 CTD following ~226°E (Figure 1). The CTD transect is supplemented by profiles collected during the mooring deployment in October 2003 (CA13) and September 2004 (CA04 and CA07) and recovery in September 2005. We also use the ArcticNet CTD data (201 stations) for 2002–2011 to compile the summer long-term mean cross-slope section following ~226°E (Figure 1a).

According to the manufacturers' estimates, individual temperature and conductivity measurements are accurate to ±0.001°C and ±0.0003 S m^{-1}, respectively, for the SBE-911, and to ±0.002°C and ±0.0003 S m^{-1}, respectively, for the SBE-37s. The temperature sensor for the ALEC is accurate to ±0.05°C. The RCM-11 Doppler Current Sensor precision and resolution are reported to be ±1% of reading and ±0.3 cm s^{-1}, respectively. The compass accuracy is ±5°. The RCM-11 temperature sensor is accurate to ±0.05°C. The accuracy of conductivity sensor is ±0.2% of range. The RDI ADCP precision and resolution are ±0.5% and ±0.1 cm s^{-1}, respectively. Its compass accuracy is ±2° and was corrected by adding magnetic deviation. The CTDs were calibrated before and after the survey.

The along-slope direction was determined by generating the scatterplot of the daily mean ADCP velocity data collected at ~8 m depth intervals over the full depth range resolved with ADCP observations—from 10 m above the ADCP transducer to the sea/ice surface (Figure 3). We assume that the along-slope flow over the Canadian Beaufort Sea continental slope is the most energetic feature of water dynamics in this region, and the maximum dispersion of velocity measurements occurs along the continental slope. Velocity dispersion attributed to baroclinicity of the water column over the slope was estimated by averaging velocity standard deviations computed for each daily-mean velocity profile. It appeared to be insignificant (Figure 3). For example, for CA-13, the along-slope variability explains ~80% of the total velocity dispersion (Figure 3c). Following this approach, the along-slope direction is aligned with the regression line describing

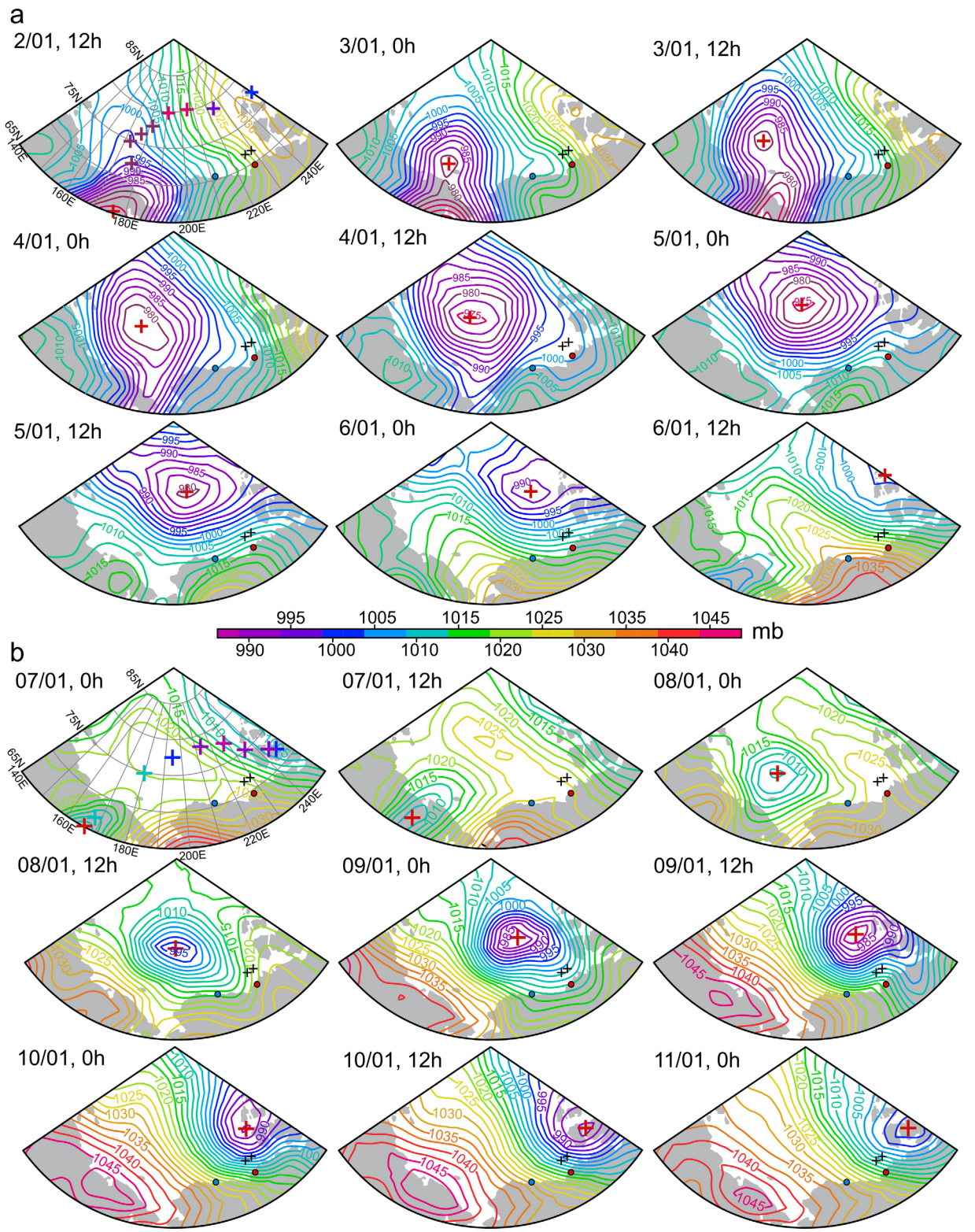

Figure 4. Sea level pressure (mb): (a) 2–6 January 2005 and (b) 7–11 January 2005 show two cyclones passing from Siberia to the Canadian Archipelago. Red crosses depict the SLP low assigned to the center of cyclone. The array of crosses in the upper left marks the cyclone pathway. Other designations are similar to that in Figure 1.

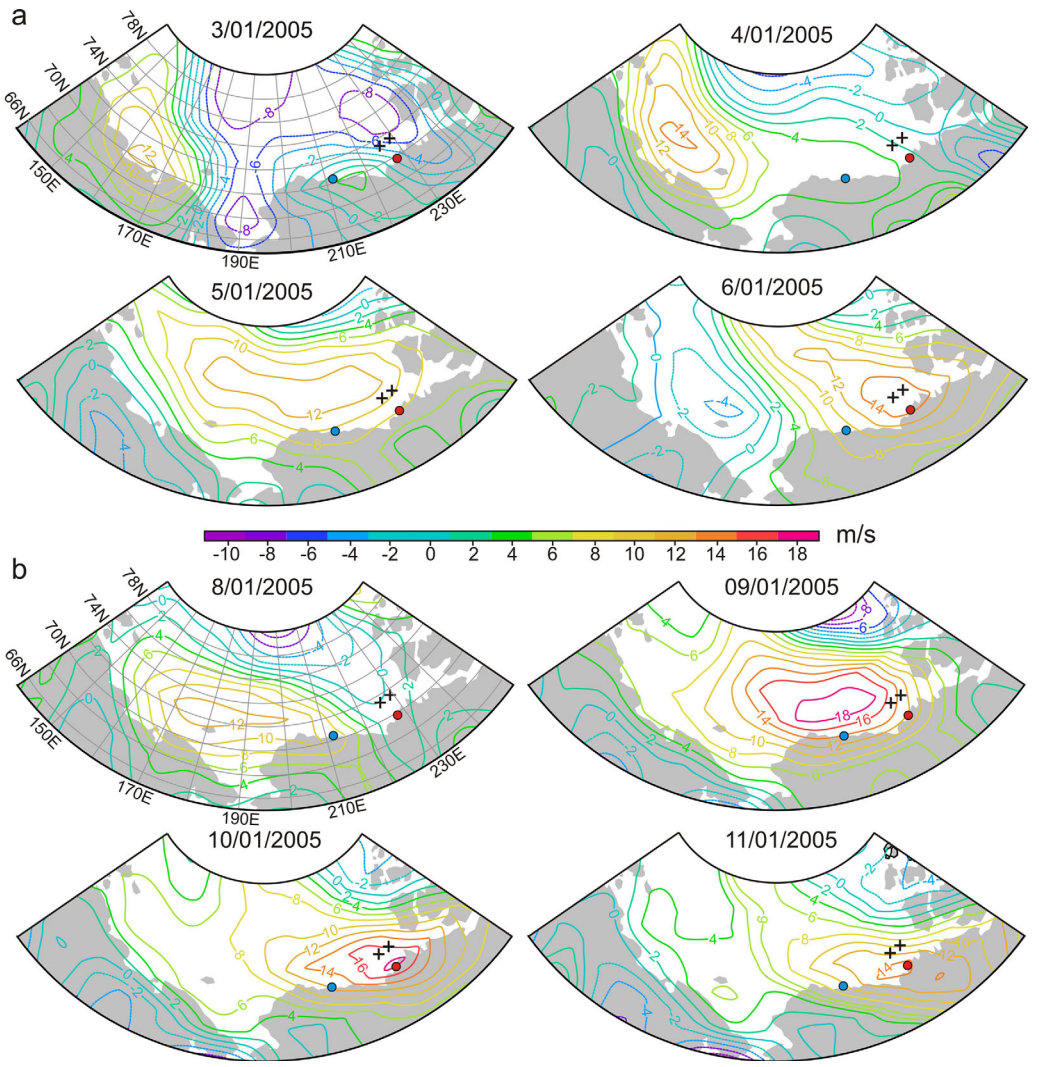

Figure 5. Zonal component of surface wind (m s^{-1}) with positive values implying westerly winds: (a) 3–6 January 2005 and (b) 8–11 January 2005. Other designations are similar to that in Figure 1.

maximum velocity dispersion. For CA04 and CA07, it was estimated as 70°T by averaging the results obtained for CA04 (68°T) and CA07 (72°T)—Figures 3a and 3b. For CA13, the along-slope direction was estimated as 64°T (Figure 3c). The 64–72°T slope direction roughly corresponds to that derived from the bottom topography (Figure 1) and reported by *Williams et al.* [2008].

For the shelfbreak current events in January 2005, the along-slope velocity of 120 cm s^{-1} was 6 times the magnitude of the cross-slope velocity. Thus, the approach we used to estimate the along-slope direction resulted in a high level of uncertainty in estimating the cross-slope velocity magnitude and sign. In the following, therefore, we primarily focus on the analysis of the along-slope velocity component.

The sea level atmospheric pressure (SLP) and 10 m winds (Figures 4 and 5, respectively) were obtained from the National Centers for Environmental Prediction (NCEP)—*Kalnay et al.* [1996]. The two cyclones at the end of December 2004 to beginning of January 2005 were tracked visually using the NCEP SLP fields, and at each time step (6 h), the position of the cyclone's center was tabulated, as was its central low SLP. The horizontal resolution of the NCEP-derived data is 2.5° of latitude.

The sea-ice concentration is derived from the Advanced Microwave Scanning Radiometer for EOS—AMSR-E and the error should not exceed 10% for concentrations above 65% [*Spreen et al.*, 2008]. The sea-ice drift is derived from the 89 GHz brightness temperature of the AMSR [*Ezraty et al.*, 2007]. The methodology used

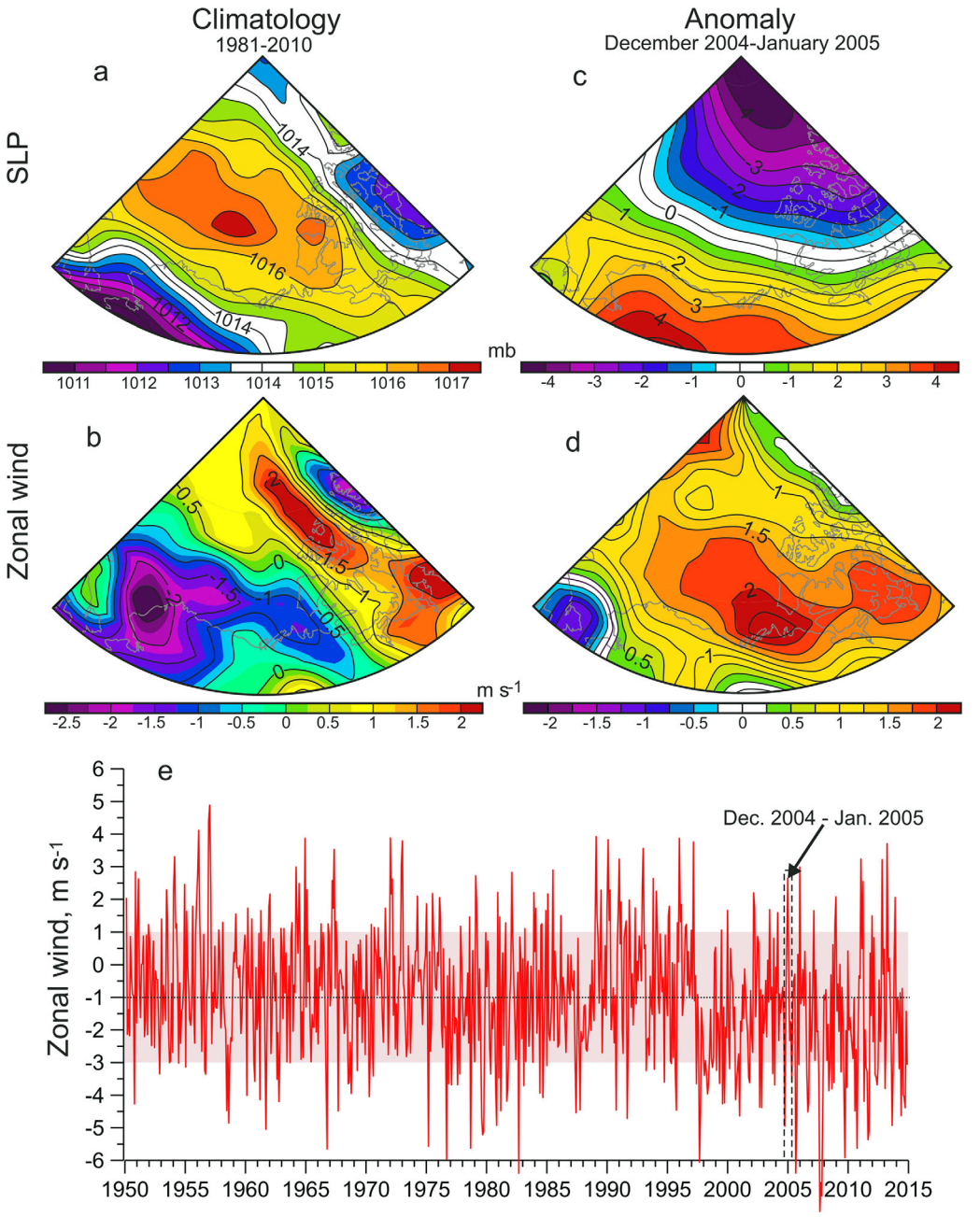

Figure 6. The NCEP-derived (a, c) sea level pressure (mb) and (b, d) zonal wind (m s^{-1}) (a, b) climatology and (c, d) anomaly associated with enhanced cyclonic activity in December 2004 to January 2005. (e) The time series of monthly mean zonal wind (m s^{-1}, the seasonal cycle was removed by subtracting the monthly mean climatology) over the mooring array shows maximum in December 2004 to January 2005 (highlighted with dashed rectangle) attributed to enhanced cyclonic activity. The pink shading depicts ±1 standard deviation of the mean shown by black dotted line.

to derive sea ice drift from AMSR-E daily brightness temperature maps is a maximum correlation method between time-lagged AMSR scenes. A time lag of 2, 3, and 6 days is used (for more details, see *Ezraty et al.* [2007]). The AMSR-E drifts compared to the trajectories of the International Arctic Buoy Program buoys over the 2002–2003 winter reveal no bias between the two independent estimates and a standard deviation of 6.7 km. The angle difference between AMSR-E and buoys shows a mean bias of 0.9° with a standard deviation of 35.2° [*Girard-Ardhuin and Ezraty*, 2005]. The spatial grid resolution for ice concentration and drift is 6.25 and 31.25 km, respectively.

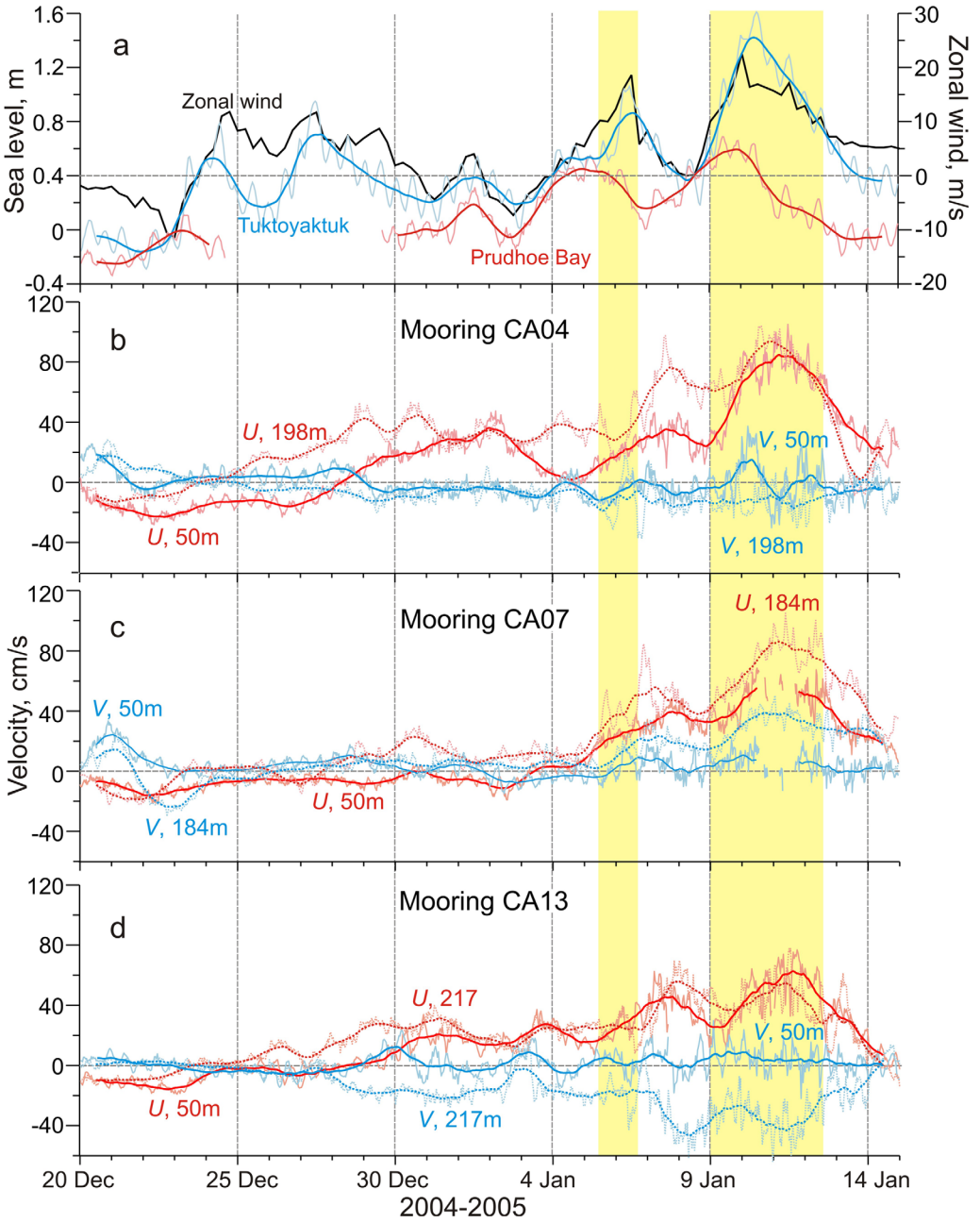

Figure 7. Time series of the (a) sea surface height (m) measured at the tide gauge in Prudhoe Bay (pink) and Tuktoyaktuk (light blue) and their 24 h running mean in red and blue, respectively, and NCEP-derived zonal wind (black, m s^{-1}) over the mooring array and (b) CA04, (c) CA07, and (d) CA13 along-slope (*U*, red) and cross-slope (*V*, blue) velocity (cm s^{-1}) at the near-surface layer (solid line) and intermediate layer (dotted line). Positive values of the along-slope and cross-slope velocities correspond to the eastward and offshore transport, respectively. Red and blue bold lines show the 24 h running mean. Yellow shading highlights two events of zonal wind exceeding 10 m s^{-1}.

For sea level records, we used the hourly tide gage data from Prudhoe Bay on the Alaskan coast and Tuktoyaktuk on the Canadian coast (Figure 1). The monthly averaged tide gauge data are corrected for (i) inverted barometer effect using atmospheric pressure from the NCEP reanalysis and (ii) glacial isostatic adjustment (GIA) using the ICE5G_VM2_L90 GIA model of *Peltier* [2004]. The seasonal cycle in monthly tide gauge records was removed by subtracting the monthly multiyear (2004–2011) mean (the monthly mean climatology). In addition, we used daily maps of SSH from AVISO (www.aviso.oceanobs.com), generated by merging multisatellite altimetry data. The high-latitude (above 66°) data are based on SARAL (operational since 2013), Cryosat-2 (operational since 2010), Envisat (operational in 2002-2012), ERS-2 (operational in

1995–2011), and ERS-1 (operational in 1991–2000) measurements. Although the separation between the satellite's ground tracks and the 35 day repeat period of SARAL, Envisat, and ERS-1/2 satellites limit the resolution of data, the convergence of the ground tracks at high latitudes provides sufficient spatial and temporal coverage to adequately resolve the mesoscale variability at high latitudes [*Volkov and Pujol*, 2012; *Volkov et al*., 2013]. Satellite altimetry data are available during summer ice-free months from June to October. To focus on the intraseasonal variability, the seasonal and interannual variability was subtracted from altimetry records. The seasonal cycle was estimated as a time series (from June to October) of the long-term (1992–2013) daily mean SSH values computed for all grid nodes where observations occurred during $\geq$10 years. The interannual variability was subtracted by removing the seasonal mean computed for every ice-free season from 1992 to 2013. Over the eastern Beaufort Sea shelf, the contribution of the seasonal and interannual variability to the total SSH variability is roughly estimated to be 25% and 32%, respectively (not shown).

3. Results

Two cyclones generated over the northeast Pacific Ocean at about 45°N, 165°E and 53°N, 163°E on 30 December 2004 and 5 January 2005, respectively, migrated over the Chukchi Peninsula toward the Chukchi Sea and then turned eastward to the Canadian Archipelago (Figure 4). These two cyclones were stalled and dissipated over the Canadian Archipelago on 7 and 12 January, respectively. On 6 and 10 January, the sea level zonal westerly wind exceeded 14 and 20 m s^{-1} at the position of the mooring array, for the first and second cyclone that passed north of the Canadian Beaufort Sea continental slope, respectively (Figures 4 and 5).

These cyclones generated significant anomalies in the SLP and zonal winds climatology. The December 2004 to January 2005 SLP anomalies show a poleward transition from positive to negative values across the southern margin of the Canada Basin (Figures 6a and 6c). This is consistent with a reversal of the atmospheric circulation over the Canada Basin from the climatic mean anticyclonic regime to a cyclonic circulation pattern that was dominant in December 2004 to January 2005. At this time, over the mooring array, the downwelling-favorable westerly wind anomaly (relative to the climate mean) reached 2.5 m s^{-1} (Figures 6b and 6d). Over the mooring array, the monthly mean westerly wind in January 2005 was 2.6 m s^{-1} exceeding standard deviation by 1.3 times (Figure 6e). In fact, the January 2005 westerly wind speed was the strongest over the entire period from January 1998 to January 2006 (Figure 6e, the seasonal cycle in monthly mean zonal wind data was removed by subtracting the monthly mean climatology). For example, on 10 January 2005, the zonal wind showed a 19 m s^{-1} anomaly relative to the NCEP climatology ($\sim$1 m s^{-1}). Overall, the 1997–2007 period showed anomalously low mean zonal wind of $-$1.8 m s^{-1} comparing to climatological mean of $-$1.0 m s^{-1}.

Following wind events on 5–6 and 9–12 January 2005, a storm surge was recorded at the Tuktoyaktuk tide gauge with a sea level rise of 1.0 m during the first and 1.5 m during the second wind events (Figure 7a). We note a similar sea level response at the Prudhoe tide gauge, caused by the same cyclones as they migrated north of the Alaskan continental slope. On 5 January and 9 January, westerly winds of up to 12 and 18 m s^{-1} caused a sea level rise at the Prudhoe tide gauge of 0.45 and 0.65 m, preceding the sea level rise at Tuktoyaktuk by 1.6 and 0.8 days, respectively (Figures 5 and 7a).

The cyclones passing over the Chukchi and Beaufort seas resulted in a reduction of sea-ice concentration. The most significant reduction (down to 70%) occurred in the Chukchi Sea on 5 and 8–9 January at the southern periphery of the cyclones where westerly wind values exceeded 12 m s^{-1} (Figures 4, 5, and 8). The second zone with low sea-ice concentrations extended over the Beaufort Sea continental slope shoreward of the cyclone pathways (Figures 4 and 8). During the strongest westerly winds over the Canadian Beaufort Sea continental slope, sea-ice reduction over the mooring array and sea level rise at Tuktoyaktuk were observed on 6 and 9–11 January (Figures 5 and 7a, and 8).

Following the first wind event, the along-slope velocity at the mooring array started to increase on 5–6 January 2005 and reached a maximum that lagged the zonal wind peak of 18 m s^{-1} by $\sim$24 h (Figure 7). During the high-flow event, the mooring lines were inclined, and the CTD-meters deepened by $\sim$10–15 m on 7 January (all moorings) and 25 m on 6 January at CA07 only (Figures 9, 10a, and 10d). At CA04, the along-slope velocity in the near-surface layer increased to 30 cm s^{-1} on 7 January at 3:00 (Figures 7b and 9a) and to 95 cm s^{-1} at 12:00 and $\sim$198 m depth (Figure 7b). At CA07 and CA13, the along-slope velocity in the

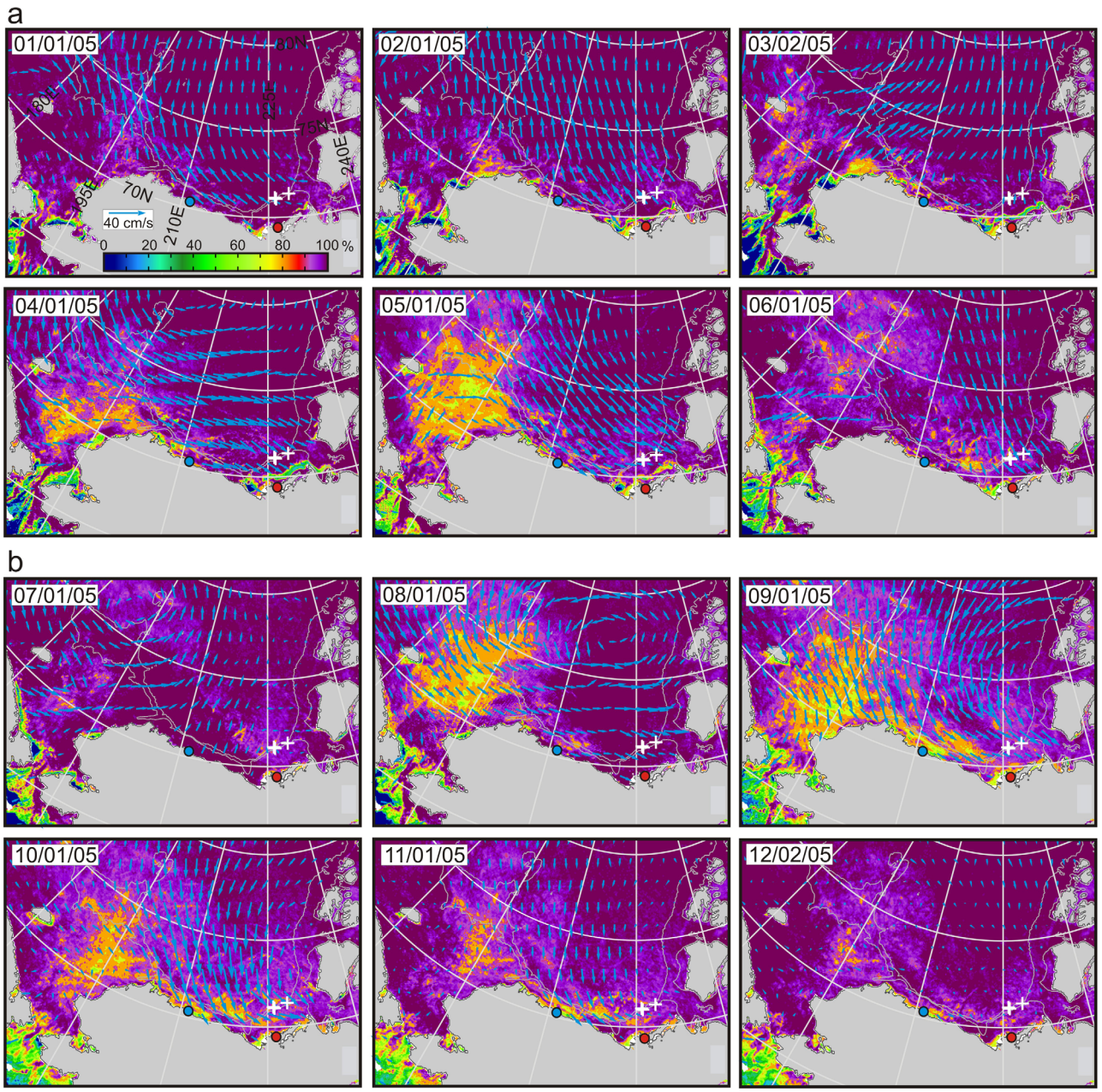

Figure 8. Sea ice concentration (%, in color) with imposed sea ice drift vectors derived from the AMSR-E satellite imagery: (a) 1–6 January 2005 and (b) 7–12 January 2005. Color and velocity scale are in the top left map. Other designations are similar to that in Figure 1.

near-surface layer increased to 25–40 and 25–30 cm s^{-1}, respectively (Figures 7c, 7d, 9c, and 9f). In the intermediate layer, the along-slope velocity increased to ~55 cm s^{-1} (Figures 7c and 7d). In addition, at CA07, the 85 cm s^{-1} velocity maximum was observed on 6 January at 23:00 and 184 m depth (Figure 7c). This velocity maximum was also recognizable in the near-surface layer (25–40 cm s^{-1}, Figure 9c) and at CA13 (from 25 to 30 cm s^{-1} in near-surface layer to 45 cm s^{-1} at ~220 m, Figures 7d and 9f). At all moorings, the along-slope flow is consistent with a depth-intensified current with velocity gradients exceeding 0.4 cm s^{-1} m^{-1} (Figures 7b–7d, 9a, 9c, and 9e).

The incline of the mooring line during the first wind event resulted in a gradual deepening of the CTDs. At CA07, a coherent *T* and *S* increase from −1.6°C and 29.6 to −1°C and 32.3, respectively, attributed to the deepening of the near-surface CTD data logger from 17 to 43 m (Figure 9c), is consistent with the

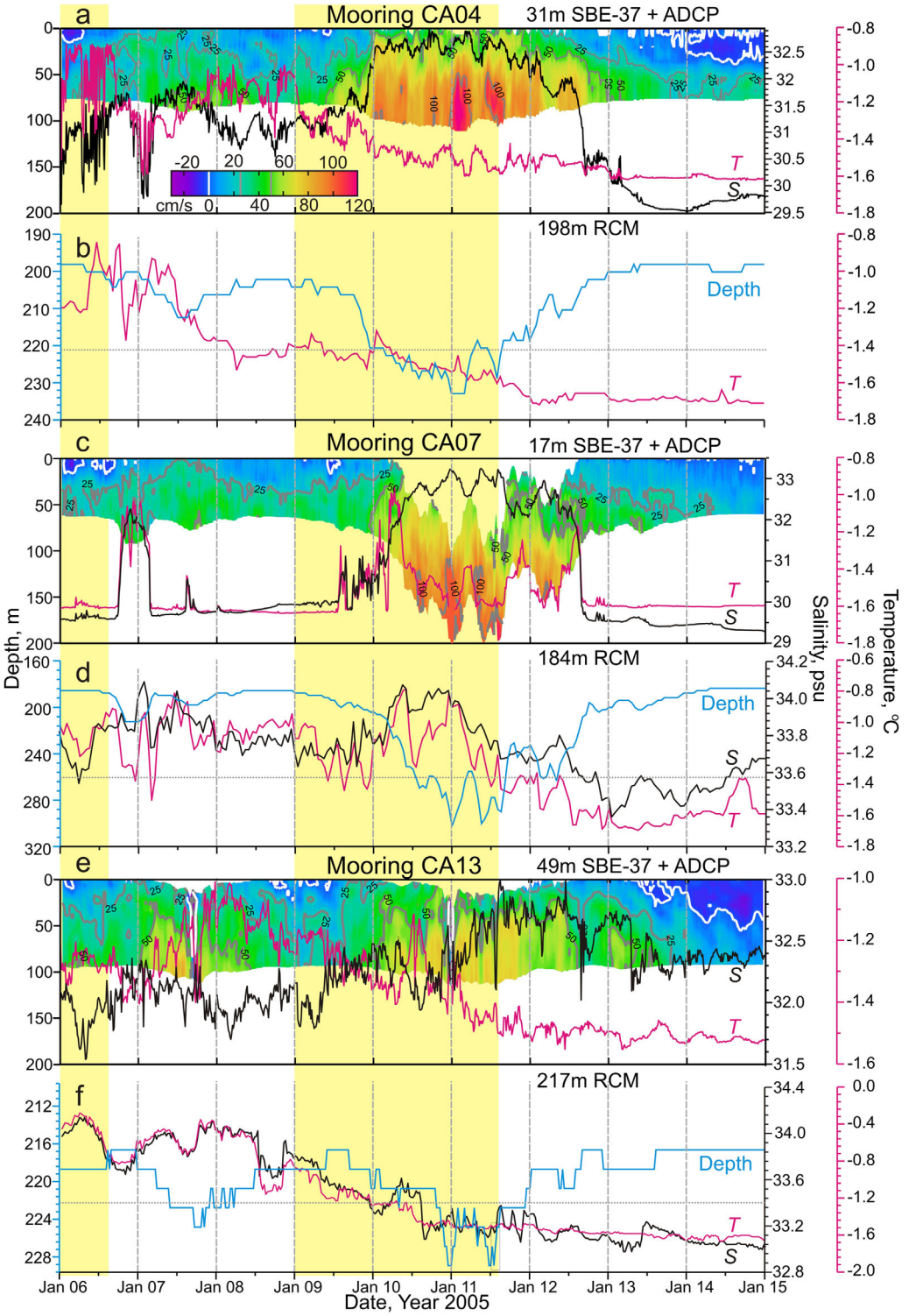

Figure 9. CTD and velocity time series at moorings CA04, CA07, and CA13 for 6–15 January 2005. (a, c, e) Along-slope velocity profiles in color (cm s^{-1}) with imposed temperature (purple, °C) and salinity (black) time series at (a) 31 m, (c) 17 m, and (e) 49 m. (b, d, f) Temperature (purple, °C), salinity (black), and depth of the instruments due to tilting of the mooring line (blue, m) time series at (b) 198 m, (d) 184 m, and (f) 217 m. Yellow shading highlights two events when zonal winds exceeded 10 m s^{-1}.

occurrence of the relatively warm near-surface layer underlying the CTD-meter. It seems that this water layer is related to the Pacific Summer Water, warmed in the Bering Sea and/or Chukchi Sea in early to mid-summer and substantially modified on its way to the mooring array site [e.g., *von Appen and Pickart*, 2012]

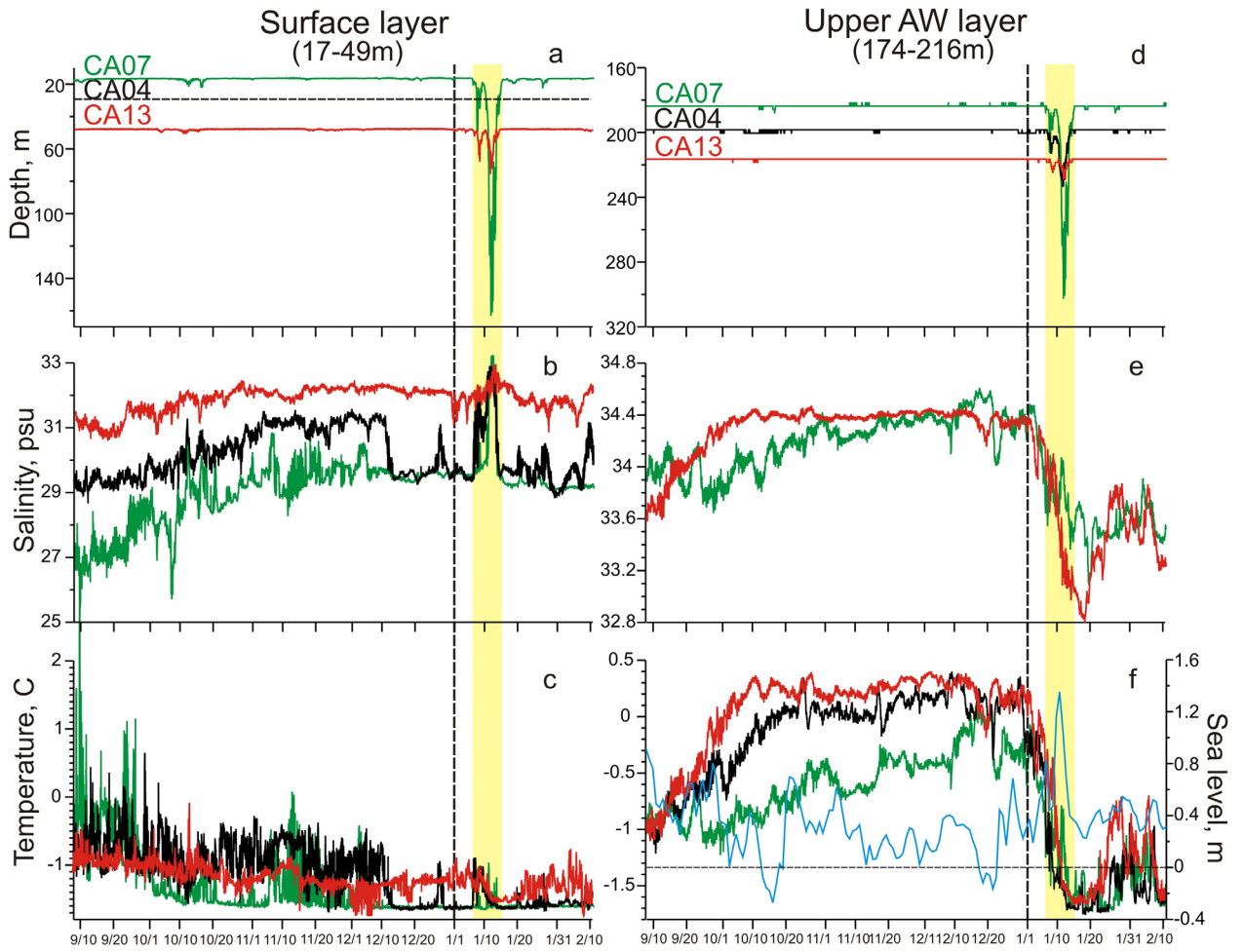

Figure 10. Time series of (a, d) depth of the instruments (m), (b, e) salinity, (c, f) temperature (°C), and (f) sea level at Tuktoyaktut (blue, m) from 8 September 2004 to 11 February 2005: (left) surface layer at CA04 (31 m, black), CA07 (17 m, green), and CA13 (49 m, red) and (right) upper AW layer at CA04 (198 m, black), CA07 (184 m, green), and CA13 (217 m, red). Note that there is no salinity data from CA04 at 198 m. Yellow shading highlights the shelfbreak current events in 6–15 January 2005. Black dashed vertical line delineates the occurrence of freshening and cooling observed in the upper AW layer (right) after 1 January 2005.

(for more details on Pacific Water, see section 4.1). However, the most significant changes in temperature and salinity were observed during the second wind event discussed below.

Following the second wind event on 9–12 January with the westerly wind velocity exceeding 20 m s^{-1} (Figure 7a), the along-slope velocity started to increase on 9 January at 12:00 almost simultaneously at CA04 and CA07 and ~3 h later at CA13 (Figures 7b–7d, 9a, 9c, and 9e.). During this event, the along-slope velocity increased from ~0 to 100 cm s^{-1} in the near-surface layer (CA04, Figures 7b and 9a) and at 75 m from 60, 25, and 40 cm s^{-1} at CA04, CA07, and CA13, respectively, up to 110 cm s^{-1} (CA04, 11 January, 3:00) (Figures 9a, 9c, and 9e), which is consistent with a depth-intensified eastward flow. In the upper Atlantic Water layer (~200 m), the along-slope velocity increased from 45 to 105 cm s^{-1} at CA04 and CA07 (Figures 7b and 7c) and from ~25 to 75 cm s^{-1} at CA13 (Figure 7d). Moreover, the second high-flow event is associated with the occurrence of a periodic component of the along-slope velocity with an amplitude of ~20 cm s^{-1} and ~10 h period (Figures 9a, 9c, and 9e). We note that this periodic signal is not coherent in time for CA04 and CA07. Rather, a 2.5 h phase shift between CA04 and CA07 is observed.

The depth-intensified along-slope eastward flow caused the mooring line to incline, which was accompanied by deepening of the near-surface CTDs by 144 and 28 m at CA07 and CA13, respectively, lasting ~2.5 days (Figure 10a). There was no pressure sensor at CA04. Because of the deepening, the CTD sensors at CA04 and CA13 measured lower temperature and greater salinity, which is consistent with CTD profiles taken during the mooring deployment and recovery (Figures 11b and 11c). At CA07, in a manner similar to

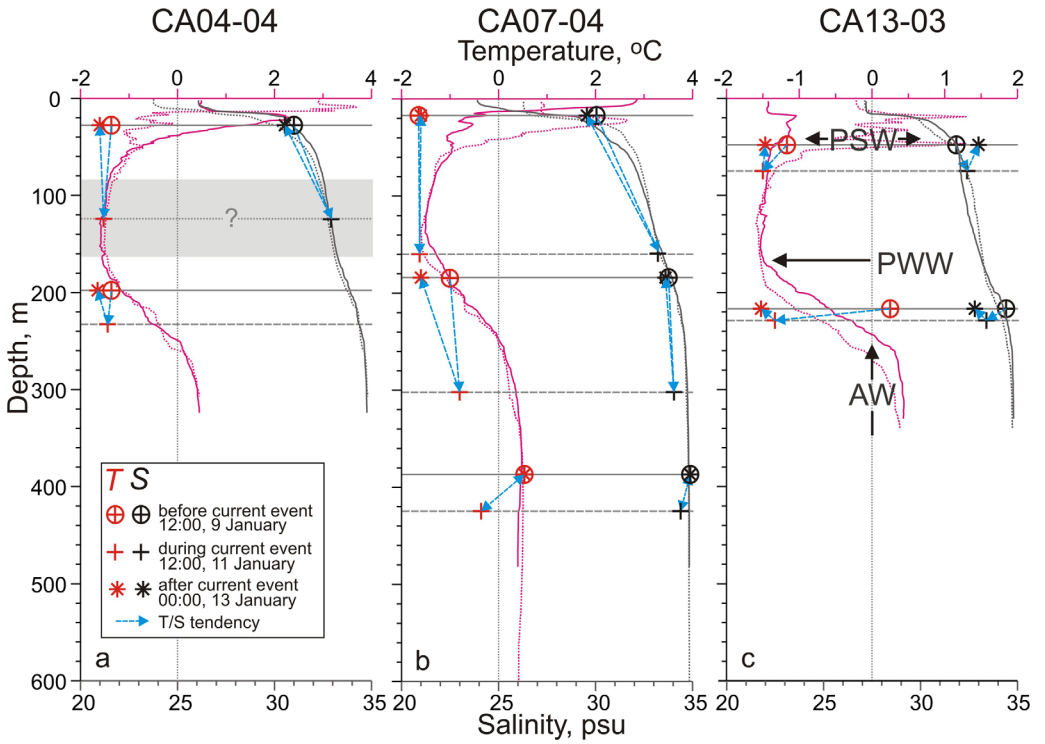

Figure 11. Vertical temperature (purple) and salinity (gray) profiles taken at mooring deployment (solid line) and recovery (dotted line) at (a) CA04, (b) CA07, and (c) CA13. Horizontal solid and dashed gray lines indicate the depth of moored CTDs before-after and during the shelfbreak current event at 9–13 January 2005 and 11 January 2005, respectively. Red and black circled crosses show temperature and salinity before the shelfbreak current event at 12:00, 9 January 2005, respectively. Red and blue crosses show temperature and salinity during the shelfbreak current event at 12:00, 11 January 2005, respectively. Red and black stars show temperature and salinity after the shelfbreak current event at 00:00, 13 January 2005, respectively. Black dashed arrows show the salinity and temperature depth tendency from 9 to 13 January 2005. (a) Horizontal dotted gray line and shading indicate the uncertain depth of the CT-meter at CA04 during the shelfbreak current event at 12:00, 11 January 2005. Black arrows highlight Pacific Summer Water (PSW), Pacific Winter Water (PWW), and Atlantic Water (AW).

the first wind event, the deepening of the near-surface CTD data logger from ~20 to 70 m resulted in greater temperature and salinity values, suggesting that there was a relatively warm layer underlying the near-surface CTD-meter (Figure 9c). At CA04, CA07, and CA13 (Figures 9b, 9d, 9f, and 10d), for ~200 m depth just above the Atlantic Water layer, the deepening of CTDs by 36, 120, and 13 m resulted in colder temperatures (by 1.1°C for CA04 and CA07 and 0.7°C for CA13) and lower salinities (by 0.7 and 1.0 for CA07 and CA13, respectively) compared to those recorded at corresponding depths during the mooring deployment and recovery (Figure 11). We note the opposite tendency of temperature and salinity relative to what one would expect from the Beaufort Sea water mass structure with warmer and saltier Atlantic Water occupying intermediate depths and causing temperature and salinity to increase below 120–160 m (Figures 11 and 12). This tendency is also consistent with CTD data from the RCM deployed at CA07 at 390 m depth (Figure 11b).

In contrast to the 390 and 17–49 m depths, temperature and salinity at 174–216 m show continuing tendency of cooling and freshening after the shelfbreak current event weakened and the CTD-meters resettled to their initial depths (Figure 11). This tendency is in line with general observation of cooling and freshening at all three moorings during 1–18 January 2005 when temperature and salinity at the upper Atlantic Water layer decreased by ~1.5°C and 1, respectively (Figure 10).

4. Discussion

4.1. Water Mass Structure

Over the Canadian Beaufort Sea continental slope, a surface layer of relatively warm and low-salinity water freshened by the Mackenzie River runoff and sea-ice melt extend across the continental slope (Figure 12). In

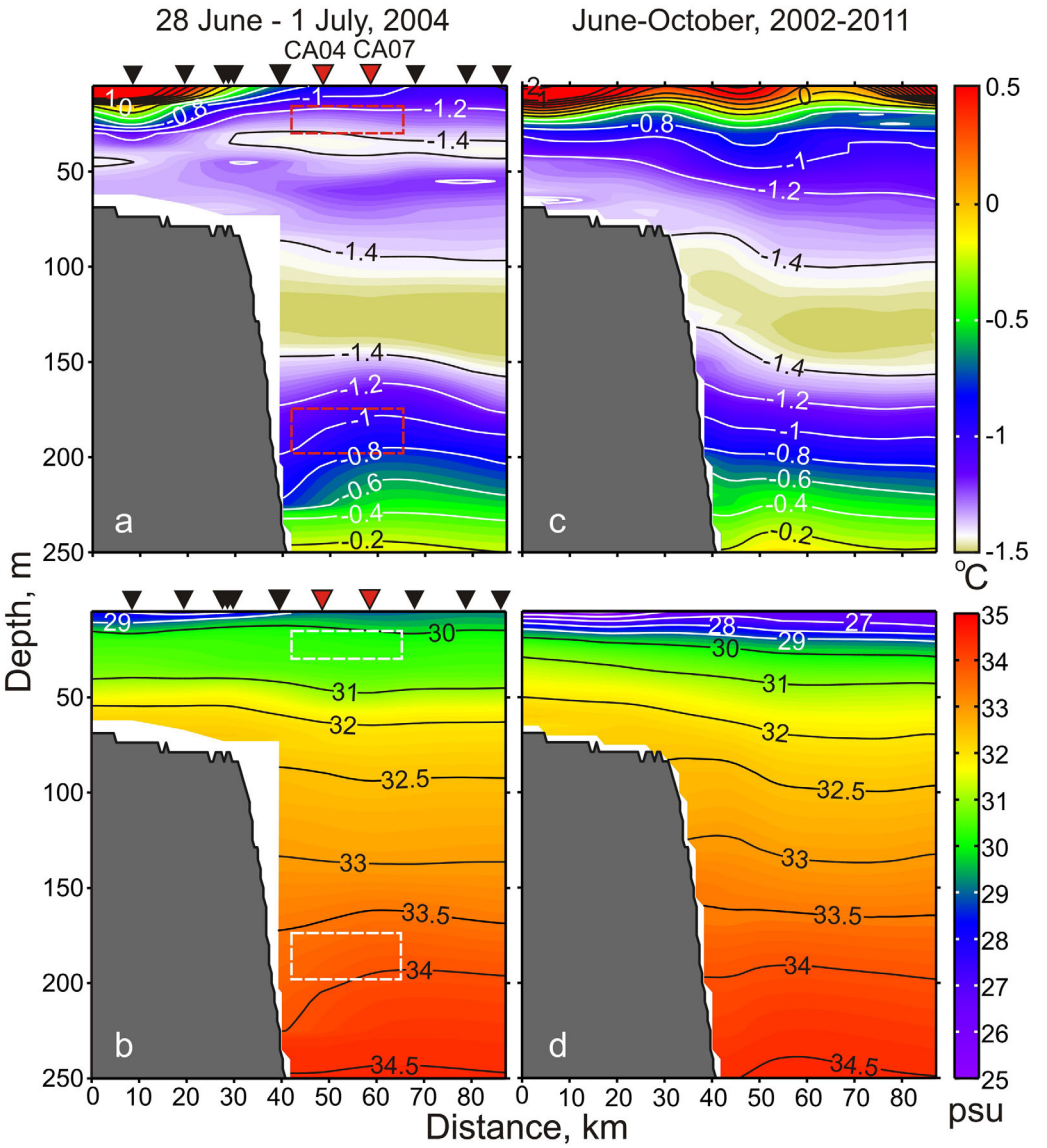

Figure 12. Cross-slope (top) temperature (°C) and (bottom) salinity transects, crossing position of moorings CA04 and CA07, (a, b) occupied from 28 June 2004 to 1 July 2004 and (c, d) compiled based on 201 ArcticNet CTD profiles collected during June–October 2002–2011. Black and red arrows at the top indicate station and mooring positions, respectively. (a, b) Dashed rectangles depict the depth range of the CTD-meters deployed at CA04 and CA07.

summer 2004, the weak temperature minimum at ~30 m is likely associated with the depth of winter convection (Figure 12a). This is consistent with a mean depth of the mixed layer in March–April reported for this area by *Peralta-Ferriz and Woodgate* [2015].

The structure of the near-surface water over the upper continental slope shown in Figures 12 and 13 is similar to that described by, e.g., *Carmack et al*. [1989], *McLaughlin et al*. [2004], and *Lansard et al*. [2012]. It is also consistent with what was reported for the Alaska Beaufort Sea slope by *Pickart* [2004], *Shimada et al*. [2005], *Nikolopoulos et al*. [2009], and *von Appen and Pickart* [2012]. Below the surface layer, the water column is comprised of water of Pacific and Atlantic origin. Water with the salinity $31 < S \leq 33$ is generally assigned to Pacific Water [*von Appen and Pickart*, 2012]. It is transported to the Beaufort Sea by the northward flow of Pacific Water emanating from Bering Strait. In this study, we associated Pacific Winter Water with the broad temperature minimum below −1.2°C centered at S ~ 33 (Figure 13b). This water is the most common winter product formed during freezing and brine rejection in the Bering and Chukchi Seas [*Weingartner et al*., 1998; *Pickart*, 2004]. Pacific Summer Water is broadly classified here as $T > -1.2$°C and

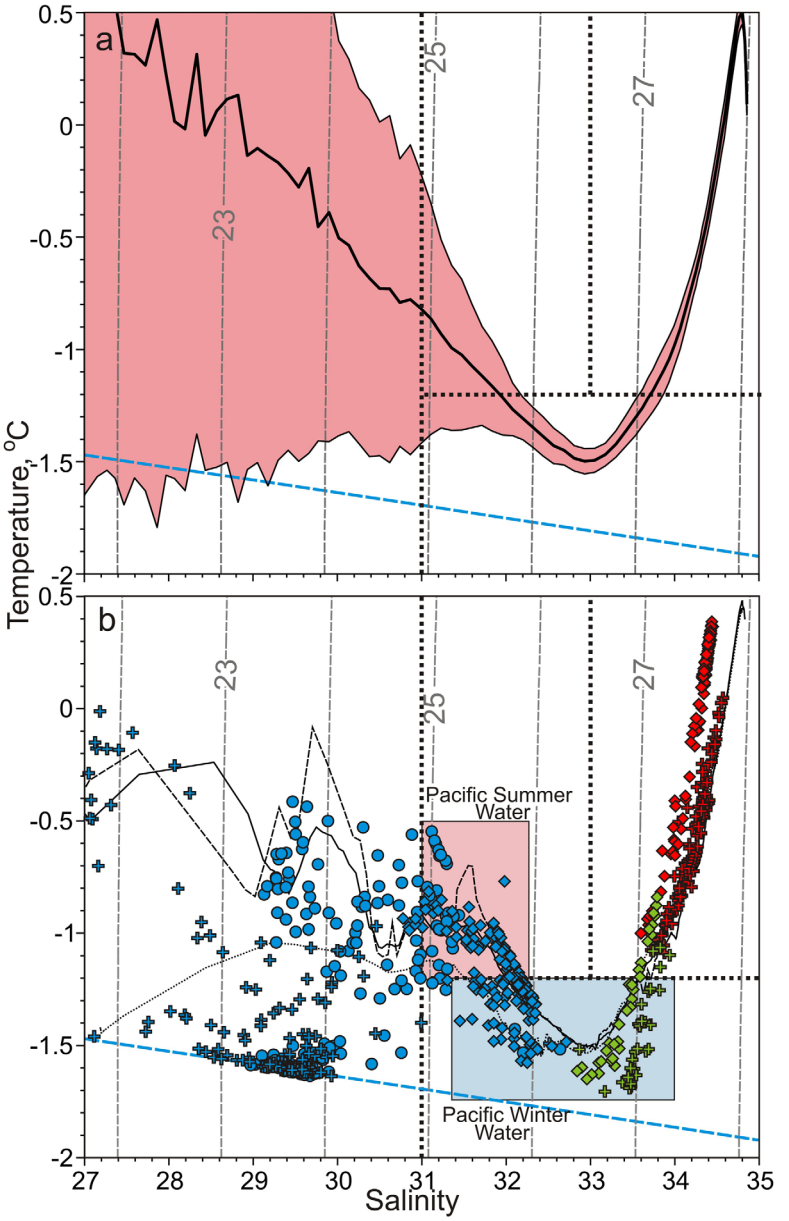

Figure 13. (a) In situ mean *TS* diagram for the cross-slope Beaufort Sea section (black). Shading depicts ±1 standard deviation. (b) The *TS* scatterplot of the daily mean temperature and salinity time series from moorings CA04 (crosses), CA07 (circles), and CA13 (diamonds). Blue and red/green symbols depict near-surface and intermediate water layer, respectively. Black dashed, solid, and dotted lines show the CTD casts taken at deployment of moorings CA04, CA07, and CA13, respectively. Pink and blue shading highlights approximate properties of Pacific Summer Water and Pacific Winter Water, respectively. Green symbols highlight a portion of record after 1 January 2015. (a, b) The gray dashed lines are σ_0 isopycnals in kg m^{-3}. The dashed blue line is surface freezing temperature. Black-dotted lines indicate the bounds defining the different water masses.

$31 < S < 32.2$ (Figure 13b). This water mass is usually comprised of the Chukchi Summer Water transported through Herald Canyon on the western Chukchi shelf [*Woodgate et al.*, 2005] and the Alaskan Coastal Water transported by the Alaskan coastal current through Barrow Canyon [*Pickart et al.*, 2005]. The warm and saltier Atlantic Water with temperatures above 0°C and $S > 33.5$ underlies Pacific Winter Water (Figure 13b).

Over the Canadian Beaufort Sea slope following ~226°E, Pacific Water occupies depths down to ~130–150 m (Figure 12d). Water as cold as −1.45°C, corresponding to Pacific Winter Water, is found offshore over the upper continental slope at ~80–160 m depths (Figures 12a and 12c). The Pacific Summer Water with temperatures of approximately −1.2°C and salinities between 31 and 32 is more prevalent inshore occupying the water column at ~50 m (Figures 12a and 12b) [e.g., *Steele et al.*, 2004; *Timmermans et al.*, 2014].

The CTD cross-slope section occupied before the mooring deployments in June–July 2004 (Figures 12a and 12b) is somewhat similar to the summer mean conditions in 2002–2011 (Figures 12c and 12d). The only principal difference in 2004 is the remaining winter cold water that overlies Pacific Summer Water at ~30–40 m (Figures 12a and 12b). Moreover, both the 2002–2011 summer mean and the summer 2004 transects are representative of the late-spring to late-summer seasonal configuration compiled by *Pickart* [2004] showing Pacific Winter Water advected in a subsurface bottom-intensified shelfbreak current. The water mass structure in Figure 12 is also generally similar to that described for the Canadian Beaufort Sea continental slope by *Carmack and Kulikov* [1998] and *Jackson et al*. [2015], and for the Canada Basin by *Jackson et al*. [2010].

The occurrence of Pacific Summer Water on the cross-slope CTD section taken in June–July 2004 (Figure 12a) is also consistent with the mooring record. At CA13, the near-surface CTD-meter at 49 m shows relatively warm mean temperatures of −1.2°C and salinity of ~31.5 (Figures 10b, 10c, and 13b). At CA07, during both storm events in January 2005, the deepening of the near-surface CTDs from ~20 to ~160 m (Figure 10a) was accompanied by a temperature increase from −1.60°C to −0.96°C (Figure 9c). It was due to a warmer Pacific Summer Water layer found below the surface cold layer, sampled by the CTD-meter at ~20 m before and after the storms. At CA04, near-surface CTD-meter at 31 m shows a mean temperature of −1°C from September to December 2004 at salinity ~30.5 (Figures 10b and 10c).

4.2. Downwelling Events and Shelfbreak Current

An important feature of salinity and density (not shown) cross-slope distribution in Figure 12 is the subsurface tilt of isohalines (isopycnals, not shown) adjacent to the upper slope. From about 30 to 130–160 m, the isohalines are sloping upward near the outer shelf and upper slope (e.g., the 32.5 contour). In contrast, in the deeper layer, they slope downward (e.g., see the 34.0 and 34.5 contours in Figures 12b and 12d). For a mean eastward flow, as reported for the Alaskan Beaufort Sea continental slope by *Pickart* [2004], *Nikolopoulos et al*. [2009], and *von Appen and Pickart* [2012], the resulting geostrophic flow is consistent with the bottom-intensified shelfbreak current with maximum velocity at the depth where the isopycnal tilt reverses. The resulting flow at CA04 during the first 2 weeks after mooring deployment in September 2004 is consistent with the CTD sections in Figure 12. At CA04 located at ~17 km from the shelfbreak, the ADCP velocity data show a depth-intensified geostrophic flow with an along-slope eastward velocity increasing from 10 cm s^{-1} in the surface layer (upper 15 m) to 15 cm s^{-1} at the shelfbreak depth of ~75 m (not shown).

During the downwelling-favorable westerly winds, as recorded on 5–6 and 9–12 January 2005 (Figures 4, 5, and 7a), the onshore Ekman transport leads to a general upward tilt of sea level that enhances the shelfbreak current velocity through the appearance of the barotropic flow component over the shelf and slope. This is consistent with the (i) velocity observations at all three moorings (Figures 7b–7d and 9), (ii) deepening of the boundary between Pacific Winter Water and Atlantic Water (Figures 9b, 9d, 9f, 10e, 10f, and 11), and (iii) two consequent storm surge events recorded by tide gauge in Prudhoe Bay and Tuktoyaktuk (Figure 7a).

However, the deepening of the boundary between Pacific Winter Water and Atlantic Water cannot be entirely attributed to the storm events of 5–6 and 9–12 January 2005. Temperature and salinity at the upper boundary of the Atlantic Water layer started to decrease on 1 January prior to the January storm events (Figures 10e, 10f, and 13b). These results suggest that the eastward flow along the Canadian Beaufort Sea continental slope was initially established in response to the downwelling-favorable wind event recorded over 24–30 December 2004 (Figure 7a). In a manner similar to the stronger events in January 2005, this wind forcing resulted in a storm surge recorded at the Tuktoyaktuk tide gauge station with a sea level rise of up to 1 m on 27 December 2004. Velocity records also show that the boundary current consistently shifted direction eastward in response to the westerly wind event on 24–30 December 2004 (Figure 7b–7d). In combination with the downwelling-favorable storms of January, this forced the subsurface Pacific Winter Water to downwell, substituting the upper Atlantic Water layer with a sharp decrease of temperature and salinity at intermediate depths from 1 to 20 January 2005 (Figure 13b). Moreover, the intermediate water became weakly stratified during downwelling (Figure 11c), suggesting that vertical mixing is strong.

Despite solid proof confirming the onshore Ekman transport over the eastern Beaufort Sea shelf in January 2005, the cross-slope velocity does not show patterns consistent with downwelling (the onshore flow in the surface layer and the compensating offshore flow in the intermediate layer)—Figures 7b–7d. This

discordance seems to be partly attributed to inaccuracies in velocity decomposition into an along-slope and cross-slope components (see section 2) allowing some portion of the along-slope velocity to appear in the cross-slope component. Moreover, numerical simulations suggest that the behavior of the compensating cross-shelf residual flow for a steady downwelling-favorable wind forcing over a uniform shelf strongly varies [*Midleton and Cirano*, 1999]. Coastally trapped waves and horizontal heterogeneity of wind forcing lead to changes in direction of the cross-shelf residual currents both in time and space. Taking into account complicated bottom topography, the coastline shape, nonstationary wind, and the presence of sea-ice, the real cross-slope flow alters considerably from one location to another.

4.3. Sea Level and Ice Variability

Satellite altimetry data over the Canadian Beaufort Sea shelf reveal an enhanced intraseasonal SSH variability over the shelf during the summer ice-free periods, with a standard deviation exceeding 8 cm (Figure 14a). This variability pattern in Figure 14a characterizes the entire Arctic shelf (not shown), and it can be explained by wind-driven effects including storm surges. Using ocean gravity measurements by GRACE twin satellites, *Volkov and Landerer* [2013] and *Peralta-Ferriz et al*. [2014] showed that on month-to-month time scales, the sea level variability over the Russian Siberian shelf is strongly related to the along shelf wind that generate the onshore Ekman transport anomalies.

Over the time interval from 2003 to 2011, the nonseasonal variability (monthly mean climatology removed) of the zonal wind stress component is significantly correlated ($r = 0.72$ at the 95% level of confidence) with the nonseasonal sea level anomalies at the Tuktoyaktuk tide gauge (Figure 14b). In particular, wind appears to be a strong driving force for the anomalies in the fall of 2007 and 2008. Overall, the largest sea level and wind stress anomalies tend to occur in fall-winter months suggesting that cross-slope SSH gradients during these months are at a maximum. The presence of sea ice can amplify the wind stress, because the ice surface provides greater drag than the open water surface [e.g., *Williams et al*., 2006; *Martin et al*., 2014]. This can also partially explain the largest SSH anomalies during fall-winter months.

The downwelling-favorable storms in January 2005 resulted in a reduction of sea-ice cover by ~20–25% observed over a relatively narrow lead stretching along the shelfbreak on 9–11 January 2005 (Figure 8). During this time, sustained reversal of the ice drift over the Beaufort Sea to cyclonic circulation occurred, and sea-ice drift over the continental slope and adjoining area was dominated by onshore and/or alongshore components (Figure 8b), suggesting that ice drift was unlikely to reduce the sea-ice concentration over the shelfbreak and continental slope. Previous studies have documented reversals of the Beaufort Gyre to cyclonic circulation due to changes in SLP and atmospheric forcing [e.g., *Lukovich and Barber*, 2006, and references therein; *Asplin et al*., 2009]. *Lukovich and Barber* [2006] demonstrated correspondence between sea ice and atmospheric vorticity. *Asplin et al*. [2009] estimated cyclonic types associated with southerly or easterly winds (favorable to Beaufort Gyre reversal, subject to the total momentum balance describing the forces that govern ice drift) to occur annually with a frequency of ~30%.

In general, low SLP results in divergence in the ice cover [e.g., *Maslanik and Barry*, 1989], the strength of which may vary depending on the persistence and location of low-pressure anomaly. In our case, however, a comparison of the locations of reduced sea ice concentration with the cyclone track (Figures 4 and 8) suggests that divergence beneath cyclones was not responsible for reduced sea ice concentration, because cyclones migrated north of the shelfbreak. The along-shelf westerly winds forced the onshore ice movement that is evident from the AMSR-E-derived ice drift vectors (Figure 8). Thus, it appears that the sea ice motion caused by the downwelling-favorable wind stress fails to explain the observed reduction of the sea-ice concentration.

It also seems likely that strains in the ice pack due to a reversal of motion in the Beaufort Sea ice gyre may fracture the pack and create conditions favorable to ice divergence [*Barry and Maslanik*, 1989]. Later studies by *Asplin et al*. [2009] have shown that cyclones control both the local divergence and convergence of sea ice through the control these storms have on the Beaufort Sea ice gyre. Leads appear at the same time as the onshore sea-ice drift (Figure 8b), which can also decrease the local sea-ice concentration through convergence of younger forms of sea ice [*Asplin et al*., 2012].

A numerical simulation of the wind-forced downwelling by *Midelton and Cirano* [1999] shows that the onshore surface Ekman transport acts to enhance the sea level gradient over the upper continental slope

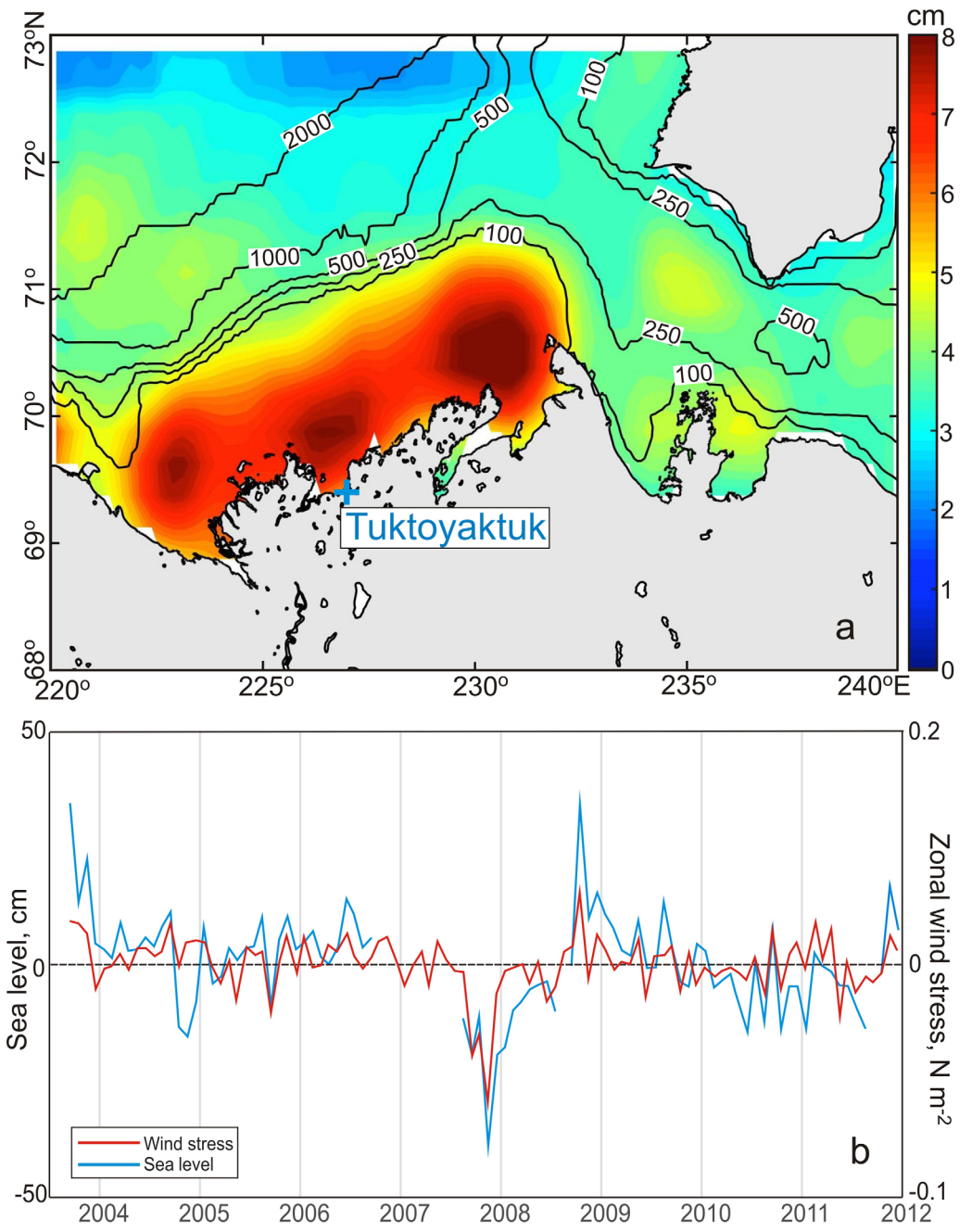

Figure 14. (a) The standard deviation of the sea surface heights (cm) from satellite altimetry for the open water season (June–October) for 1992–2013 (seasonal and interannual variability removed). Black numbered lines show bottom topography (m). (b) The monthly time series of sea level anomaly at Tuktoyaktuk tide gauge (blue) and NCEP zonal wind stress (red) averaged over the area 220°E–235°E and 70°N–72.5°N. The tide gauge data are corrected for inverted barometer and glacial isostatic adjustment (GIA) using the ICE5G_VM2_L90 GIA model [*Peltier*, 2004]. The seasonal cycle is removed from all time series.

between ~100 and 300 m depth. We also note that reduced sea-ice concentration on 9–11 January is coincident with the maximum storm surge at Prudhoe Bay and Tuktoyaktuk tide gauges (Figure 7a). The above considerations allow us to hypothesize that the sea-ice dynamics over the continental slope can be partly controlled by the cross-slope SSH gradient enhanced during the winter downwelling-favorable storms. This also follows from the ice momentum equation that includes forcing from the atmosphere-ice and ocean-ice stresses, and the sea surface height gradient [e.g., *Schmidt et al.*, 2004]. A further and more detailed investigation involving numerical simulations and high-resolution AMSR-2 imagery [e.g., *Beitsch et al.*, 2014] is

necessary to advance our understanding of sea-ice dynamics associated with the winter downwelling-favorable storms.

5. Conclusions

We investigated the ocean response to two consecutive downwelling-favorable winter storms with westerly winds exceeding 20 m s^{-1}over the continental slope of the Canadian Beaufort Sea.

In January 2005, two Pacific-born cyclones passed north of the Beaufort Sea continental slope toward the Canadian Archipelago where they were stalled and dissipated. The Coriolis force and frictional coupling of wind, ice, and water caused an onshore Ekman transport of surface water that generated a storm surge along the Beaufort Sea coast with SSH increasing up to 1.5 m following two westerly wind maxima. Three oceanographic moorings deployed over the upper continental slope at 300–500 m depth simultaneously recorded two consecutive shelfbreak current events with an along-slope eastward depth-intensified flow of up to ~80 and 120 cm s^{-1} for the first event on 7 January and second event on 10–11 January, respectively, representing one of the strongest depth-intensified, subtidal flows recorded in the Canadian Arctic.

The elevated SSH over the shelf produces a pressure gradient, which was directed normal to the coast. This gradient drives a geostrophic current along the continental slope, in the same direction as the wind. This along-slope eastward barotropic flow was superimposed to the background baroclinic depth-intensified shelfbreak current, significantly enhancing the along-slope eastward transport established in response to the preceding downwelling-favorable wind event in December 2004. We suggest that this mechanism explains the observed shelfbreak current events described in this paper.

In addition, we suggest that the along-slope wind induced a continental slope downwelling, i.e., a downward water movement in response to the surface onshore Ekman transport, although the flow at the intermediate depths shows no consistent off-slope compensating transport. The fixed-depth CTDs at all three moorings recorded a deepening boundary between the Pacific Winter Water and the Atlantic Water. However, it seems that the downwelling was not entirely attributed to the January storm events. The boundary current consistently shifted direction eastward in response to westerly winds during a preceding storm event on 24–30 December 2004. This storm event was also associated with the onset of downwelling.

Summer satellite altimetry data show that the largest intraseasonal SSH variability is observed over the shelf, probably in response to frequent storm surges. This leads to enhanced SSH gradients over the upper continental slope. We hypothesize that during winter this may lead to a reduction of sea-ice cover over the upper continental slope as we observed in January 2005.

It should be noted that the mooring array was about 20–30 km north of the shelfbreak (Figure 1), and this seems to be the reason why moorings did not record the consistent eastward shelfbreak flow during the entire period of observations (Figure 3) as reported by *Forest et al*. [2015] for a mooring deployed ~4 km off the shelf edge. We also note that our analysis is strongly limited by the availability of CTD data, obtained only at some distinct depth levels. The deficiency of this analysis, particularly the lack of consistent off-slope compensating transport during downwelling, clearly defines a necessity for further research in this area based on a representative mooring array crossing the continental slope, similar to that conducted over the Alaskan continental slope (Figure 1) [e.g., *Nikolopoulos et al*., 2009; *von Appen and Pickart*, 2012]. Modeling efforts are also necessary to investigate the sea-ice dynamics associated with winter downwelling-favorable storms. Finally, our research points toward several topics for future investigation. Of particular interest are the links between SSH to reduced ice concentration and using sea-ice concentration as proxies for the coastal downwelling.

Acknowledgments
The data used for this research were collected under the ArcticNet framework, project Long-Term Oceanic Observatories in the Canadian Arctic. We gratefully acknowledge the support by the Canada Excellence Research Chair (CERC) and the Canada Research Chairs (CRC) programs. This work is a contribution to the joint Canadian-Danish-Greenland ASP cooperation. The research was also partly supported by National Sciences and Engineering Research Council of Canada (NSERC, grant RGPIN-2014-03606) and the base funds of NOAA Atlantic Oceanographic and Meteorological Laboratory. The CTD and velocity data are available through the Polar Data Catalogue at https://www.polardata.ca/pdcsearch/, CCIN Reference #11653 and #11792. The SSH data were produced by Ssalto/Duacs and distributed by Aviso (www.aviso.oceanobs.com) with support from CNES.

References

Asplin, M. G., J. V. Lukovich, and D. G. Barber (2009), Atmospheric forcing of the Beaufort Sea Ice Gyre: Surface pressure climatology and sea ice motion, *J. Geophys. Res.*, *114*, C00A06, doi:10.1029/2008JC005127.

Asplin, M. G., R. Galley, D. G. Barber, and S. Prinsenberg (2012), Fracture of summer perennial sea ice by ocean swell as a result of Arctic storms, *J. Geophys. Res.*, *117*, C06025, doi:10.1029/2011JC007221.

Barber, D. G., et al. (2015), Selected physical, biological and biogeochemical implications of a rapidly changing Arctic Marginal Ice Zone, *Prog. Oceanogr.*, *139*, 122–150, doi:10.1016/j.pocean.2015.09.003.

Barry, R. G., and J. Maslanik (1989), Arctic sea ice characteristics and associated atmosphere-ice interactions in summer inferred from SMMR data and drifting buoys: 1979-1984, *GeoJournal*, *18*(1), 35–44.
Beitsch, A., L. Kaleschke, and S. Kern (2014), Investigating high-resolution AMSR2 sea ice concentrations during the February 2013 Fracture Event in the Beaufort Sea, *Remote Sensing*, *6*(5), 3841–3856, doi:10.3390/rs6053841.
Carmack, E. C., and E. A. Kulikov (1998), Wind-forced upwelling and internal Kelvin wave generation in Mackenzie Canyon, Beaufort Sea, *J. Geophys. Res.*, *103*(C9), 18,447–18,458.
Carmack, E. C., R. W. Macdonald, and J. E. Papadakis (1989), Water mass structure and boundaries in the Mackenzie shelf estuary, *J. Geophys. Res.*, *94*(C12), 18,043–18,055, doi:10.1029/JC094iC12p18043.
Ezraty, R., F. Girard-Ardhuin, and D. Croizé-Fillon (2007), *Sea Ice Drift in the Central Arctic Using the 89 GHz Brightness Temperatures of the Advanced Microwave Scanning Radiometer, User's Manual*, IFREMER, Brest, France.
Forest, A., P. D. Osborne, L. Fortier, M. Sampei, and M. G. Lowings (2015), Physical forcings and intense shelf–slope fluxes of particulate matter in the halocline waters of the Canadian Beaufort Sea during winter, *Cont. Shelf Res.*, *101*, 1–21.
Girard-Ardhuin, F., and R. Ezraty (2005), Validation of Arctic sea ice drift with IABP buoys, paper presented at Satellite Application Facility training Workshop, Ocean and Sea Ice Second Workshop, Perros-Guirec, France, 15–17 March.
Hudak, D. R., and J. M. C. Young (2002), Storm climatology of the Southern Beaufort Sea, *Atmos. Ocean*, *40*(2), 145–158, doi:10.3137/ao.400205.
Jackson, J. M., E. C. Carmack, F. A. McLaughlin, S. E. Allen, and R. G. Ingram (2010), Identification, characterization, and change of the near-surface temperature maximum in the Canada Basin, 1993–2008, *J. Geophys. Res.*, *115*, C05021, doi:10.1029/2009JC005265.
Jackson, J. M., H. Melling, J. V. Lukovich, D. Fissel, and D. G. Barber (2015), Formation of winter water on the Canadian Beaufort shelf: New insight from observations during 2009–2011, *J. Geophys. Res. Oceans*, *120*, 4090–4107, doi:10.1002/2015JC010812.
Jones, E. P., L. G. Anderson, and J. H. Swift (1998), Distribution of Atlantic and Pacific waters in the upper Arctic Ocean: Implications for circulation, *Geophys. Res. Lett.*, *25*(6), 765–768.
Jones, E. P., J. H. Swift, L. G. Anderson, M. Lipizer, G. Civitarese, K. K. Falkner, G. Kattner, and F. A. McLaughlin (2003), Tracing Pacific water in the North Atlantic Ocean, *J. Geophys. Res.*, *108*(C4), 3116, doi:10.1029/2001JC001141.
Kalnay, E., et al. (1996), The NCEP/NCAR 40-year reanalysis project, *Bull. Am. Meteorol. Soc.*, *77*, 437–471, doi:10.1175/1520-0477(1996)077<0437:TNYRP>2.0.CO;2.
Kulikov, E. A., E. C. Carmack, and R. W. Macdonald (1998), Flow variability at the continental shelf break of the Mackenzie Shelf in the Beaufort Sea, *J. Geophys. Res.*, *103*(C6), 12,725–12,741.
Lansard, B., A. Mucci, L. A. Miller, R. W. Macdonald, and Y. Gratton (2012), Seasonal variability of water mass distribution in the southeastern Beaufort Sea determined by total alkalinity and $\delta^{18}O$, *J. Geophys. Res.*, *117*, C03003, doi:10.1029/2011JC007299.
Lukovich, J. V., and D. G. Barber (2006), Atmospheric controls on sea ice motion in the southern Beaufort Sea, *J. Geophys. Res.*, *111*, D18103, doi:10.1029/2005JD006408.
Martin, T., M. Steele, and J. Zhang (2014), Seasonality and long-term trend of Arctic Ocean surface stress in a model, *J. Geophys. Res. Oceans*, *119*, 1723–1738, doi:10.1002/2013JC009425.
Maslanik, J. A., and R. G. Barry (1989), Short-term interactions between atmospheric synoptic conditions and sea ice behavior in the Arctic, *Ann. Glaciol.*, *12*, 113–117.
McLaughlin, F., E. Carmack, R. Macdonald, A. J. Weaver, and J. Smith (2002), The Canada Basin, 1989–1995: Upstream events and far-field effects of the Barents Sea, *J. Geophys. Res.*, *107*(C7), 3082, doi:10.1029/2001JC000904.
McLaughlin, F. A., E. C. Carmack, R. W. MacDonald, H. Melling, J. H. Swift, P. A. Wheeler, B. F. Sherr, and E. B. Sherr (2004), The joint roles of Pacific and Atlantic-origin waters in the Canada Basin, 1997–1998, *Deep Sea Res., Part I*, *51*, 107–128.
Melling, H. (1993), The formation of a haline shelf front in wintertime in an ice-covered arctic sea, *Cont. Shelf Res.*, *13*, 1123–1147.
Midleton, J. F., and M. Cirano (1999), Wind-forced downwelling slope currents: A numerical study, *J. Phys. Oceanogr.*, *29*, 1723–1743.
Nikolopoulos, A., R. S. Pickart, P. S. Fratantoni, K. Shimada, D. J. Torres, and E. P. Jones (2009), The western Arctic boundary current at 152°W: Structure, variability, and transport, *Deep Sea Res., Part II*, *56*, 1164–1181, doi:10.1016/j.dsr2.2008.10.014.
Peltier, W. R. (2004), Global glacial isostasy and the surface of the Ice-Age Earth: The ICE-5G(VM2) model and GRACE, *Annu. Rev. Earth Planet. Sci.*, *32*, 111–149, doi:10.1146/annurev.earth.32.082503.144359.
Peralta-Ferriz, C., and R. A. Woodgate (2015), Seasonal and interannual variability of pan-Arctic surface mixed layer properties from 1979 to 2012 from hydrographic data, and the dominance of stratification for multiyear mixed layer depth shoaling, *Prog. Oceanogr.*, *134*, 19–53, doi:10.1016/j.pocean.2014.12.005.
Peralta-Ferriz, C., J. H. Morison, J. M. Wallace, J. A. Bonin, and J. Zhang (2014), Arctic Ocean circulation patterns revealed by GRACE, *J. Clim.*, *27*, 1445–1468, doi:10.1175/JCLI-D-13-00013.1.
Pickart, R. S. (2004), Shelfbreak circulation in the Alaskan Beaufort Sea: Mean structure and variability, *J. Geophys. Res.*, *109*, C04024, doi:10.1029/2003JC001912.
Pickart, R. S., T. J. Weingartner, L. J. Pratt, S. Zimmermann, and D. J. Torres (2005), Flow of winter-transformed Pacific water into the western Arctic, *Deep Sea Res., Part II*, *52*, 3175–3198.
Pickart, R. S., G. W. K. Moore, D. J. Torres, P. S. Fratantoni, R. A. Goldsmith, and J. Yang (2009), Upwelling on the continental slope of the Alaskan Beaufort Sea: Storms, ice, and oceanographic response, *J. Geophys. Res.*, *114*, C00A13, doi:10.1029/2008JC005009.
Pickart, R. S., M. A. Spall, G. W. K. Moore, T. J. Weingartner, R. A. Woodgate, K. Aagaard, and K. Shimada (2011), Upwelling in the Alaskan Beaufort Sea: Atmospheric forcing and local versus non-local response, *Prog. Oceanogr.*, *88*, 78–100, doi:10.1016/j.pocean.2010.11.005.
Pickart, R. S., M. A. Spall, and J. T. Mathis (2013a), Dynamics of upwelling in the Alaskan Beaufort Sea and associated shelf–basin fluxes, *Deep Sea Res., Part I*, *76*, 35–51, doi:10.1016/j.dsr.2013.01.007.
Pickart, R. S., L. M. Schulze, G. W. K. Moore, M. A. Charette, K. R. Arrigo, G. Dijken, and S. L. Danielson (2013b), Long-term trends of upwelling and impacts on primary productivity in the Alaskan Beaufort Sea, *Deep Sea Res., Part I*, *79*, 106–121, doi:10.1016/j.dsr.2013.05.003.
Rudels, B., E. P. Jones, L. G. Anderson, and G. Kattner (1994), On the intermediate depth waters of the Arctic Ocean, in *The Polar Oceans and Their Role in Shaping the Global Environment: The Nansen Centennial Volume, Geophys. Monogr. Ser.*, vol. 85, edited by O. M. Johannessen, R. D. Muench, and J. E. Overland, pp. 33–46, AGU, Washington, D. C.
Rudels, B., E. P. Jones, U. Schauer, and P. Eriksson (2004), Atlantic sources of the Arctic Ocean surface and halocline waters, *Polar Res.*, *23*(2), 181–208.
Schmidt, G. A., C. M. Bitz, U. Mikolajewicz, and L.-B. Tremblay (2004), Ice-ocean boundary conditions for coupled models, *Ocean Modell.*, *7*, 59–74, doi:10.1016/S1463-5003(03)00030-1.
Schulze, L. M., and R. S. Pickart (2012), Seasonal variation of upwelling in the Alaskan Beaufort Sea: Impact of sea ice cover. *J. Geophys. Res.*, *117*, C06022, doi:10.1029/2012JC007985.

Serreze, M. C., and A. P. Barrett (2011), Characteristics of the Beaufort Sea High, *J. Clim.*, *24*, 159–182, doi:10.1175/2010JCLI3636.1.
Shimada, K., M. Itoh, S. Nishino, F. McLaughlin, E. Carmack, and A. Proshutinsky (2005), Halocline structure in the Canada Basin of the Arctic Ocean, *Geophys. Res. Lett.*, *32*, L03605, doi:10.1029/2004GL021358.
Spreen, G., L. Kaleschke, and G. Heygster (2008), Sea ice remote sensing using AMSR-E 89 GHz channels, *J. Geophys. Res.*, *113*, C02S03, doi:10.1029/2005JC003384.
Steele, M., J. Morison, W. Ermold, I. Rigor, M. Ortmeyer, and K. Shimada (2004), Circulation of summer Pacific halocline water in the Arctic Ocean, *J. Geophys. Res.*, *109*, C02027, doi:10.1029/2003JC002009.
Timmermans, M.-L., et al. (2014), Mechanisms of Pacific summer water variability in the Arctic's Central Canada Basin, *J. Geophys. Res. Oceans*, *119*, 7523–7548, doi:10.1002/2014JC010273.
Volkov, D. L., and F. W. Landerer (2013), Nonseasonal fluctuations of the Arctic Ocean mass observed by the GRACE satellites, *J. Geophys. Res. Oceans*, *118*, 6451–6460, doi:10.1002/2013JC009341.
Volkov, D. L., and M.-I. Pujol (2012), Quality assessment of a satellite altimetry data product in the Nordic, Barents, and Kara Seas, *J. Geophys. Res.*, *117*, C03025, doi:10.1029/2011JC007557.
Volkov, D. L., T. V. Belonenko, and V. R. Foux (2013), Puzzling over the dynamics of the Lofoten Basin—A sub-Arctic hot spot of ocean variability, *Geophys. Res. Lett.*, *40*, 738–743, doi:10.1002/grl.50126.
von Appen, W.-J., and R. S. Pickart (2012), Two configurations of the Western Arctic Shelfbreak current in summer, *J. Phys. Oceanogr.*, *42*, 329–351, doi:10.1175/JPO-D-11-026.1.
Weingartner, T., D. Cavalieri, K. Aagaard, and Y. Sasaki (1998), Circulation, dense water formation, and outflow on the northeast Chukchi shelf, *J. Geophys. Res.*, *103*(C4), 7647–7661.
Williams, W. J., E. C. Carmack, K. Shimada, H. Melling, K. Aagaard, R. W. Macdonald, and R. G. Ingram (2006), Joint effects of wind and ice motion in forcing upwelling in Mackenzie Trough, Beaufort Sea, *Cont. Shelf Res.*, *26*, 2352–2366, doi:10.1016/j.csr.2006.06.012.
Williams, W. J., H. Melling, E. C. Carmack, and R. G. Ingram (2008), Kugmallit Valley as a conduit for cross-shelf exchange on the Mackenzie shelf in the Beaufort Sea, *J. Geophys. Res.*, *113*, C02007, doi:10.1020/2006JC003591.
Woodgate, R. A., K. Aagaard, and T. J. Weingartner (2005), Monthly temperature, salinity, and transport variability of the Bering Strait through flow, *Geophys. Res. Lett.*, *32*, L04601, doi:10.1029/2004GL021880.
Yang, J. (2009), Seasonal and interannual variability of downwelling in the Beaufort Sea, *J. Geophys. Res.*, *114*, C00A14, doi:10.1029/2008JC005084.